On the evaluation of the Wendelstein experiments

G. v.Gierke, G. Grieger,
K.U. von Hagenow

2/70 July 1968

INSTITUT FÜR PLASMAPHYSIK
GARCHING BEI MÜNCHEN

INSTITUT FÜR PLASMAPHYSIK

GARCHING BEI MÜNCHEN

On the evaluation of the Wendelstein experiments

G. v.Gierke, G. Grieger,
K.U. von Hagenow

2/70 July 1968

Die nachstehende Arbeit wurde im Rahmen des Vertrages zwischen dem Institut für Plasmaphysik GmbH und der Europäischen Atomgemeinschaft über die Zusammenarbeit auf dem Gebiete der Plasmaphysik durchgeführt.

IPP 2/70

G. von Gierke
G. Grieger
K.U. von Hagenow

On the evaluation of the Wendelstein experiments

July 1968 (in English)

Abstract

The earlier evaluations of the experiments performed in 1965 in the Wendelstein stellarator W Ib have been revised. In particular, later probe calibrations by Hashmi et.al., the shape of the magnetic surfaces and the magnitude of the rotational transform as obtained by means of a pulsed electron beam have been taken into account. The results are compared with numerical calculations based upon a simple model assuming resistive diffusion modified for stellarator geometry and recombination on the surfaces of the emitter and the probes. The time dependence of the temperature of the emitter and the elliptical shape of the cross sections of the magnetic surfaces is also considered.

The measured peak ion densities and even their dependence on time agree fairly well with the calculations as long as ion inertia can be neglected. Equilibrium breaks down if the required velocity of the balancing mass flow (which is necessary for stellarator equilibrium) exceeds about the ion thermal velocity. In the transition region estimates taking into account the effect of ion inertia seem to show agreement with the observations.

Introduction

The experiments with Cs plasma obtained by contact ionization and its diffusion across the magnetic field of the stellarator Wendelstein W Ib represent a complicated synthesis of investigations on Q-machines and stellarators. Without the understanding of the physics of both confinement schemes a discussion of the results is impossible.

The only aim of the earlier experiments was to investigate whether the plasma losses are governed by "Bohm diffusion" in this device, or, as it finally could be reported at the Culham Conference [1], could be described on the basis of resisitve diffusion and recombination on the surfaces of the emitter, supports and probes. In the next series of experiments [2] we tried to reduce the loss rate due to surface recombination by such an extent that diffusion becomes the predominant or at least a comparable loss process.With the diagnostic techniques available at that time this intention required a strong restriction in the accessible information.

Furthermore, also in this experiment it was not the aim to determine the exact value of the diffusion coefficient, as it was clear that this would require both more refined diagnostic tools and, for comparison with the experimental results, complicated calculations. But we wanted to show that in a range of parameters where resistive and Bohm diffusion differ by orders of magnitude, the loss rates and their dependences on different parameters roughly agree with a simple model based only on classical assumptions. We were and are still convinced that steady state experiments are easier to evaluate, but in this report the time dependent behaviour shall also be investigated.

We have to thank W. Stodiek for his criticism which initiated a revision of our earlier evaluation and explanation of the experimental results. Along this way several new corrections have been introduced. New information was gained from a measurement of the magnetic surfaces in W Ib by means of a pulsed electron beam [3].

A refined but still comparatively simple model is used for the calculations.

The stellarator as Q-machine

S.v.Goeler has given an "equilibrium model"[4] for a Q-machine which allows to calculate all particle fluxes existing in this device. This model can also be applied to the central region of a stellarator where the plasma is produced by contact ionization.

In one respect the stellarator is even a better Q-device as illustrated in fig. 1. The usual Q-machine has three regions with different physical properties. Region a) the region determined by the parts of the emitter which are illuminated by the atomic beam. There the plasma properties depend on density and temperature but are independent of the properties of the emitter, at least theoretically if the plasma would be in equilibrium. Region b) which region is determined by the parts of the emitter not being illuminated by the neutral beam. There the plasma is governed by diffusion parallel and perpendicular to the magnetic field and recombination on the surface of the emitter depending only slightly on the emitter properties. Region c) which is beyond the edge of the emitter and subject to a large recombination on the cold ends of the device. So only regions a and b are accessible to meaningful experimental investigations.

In a stellarator however, the region a) is determined by a nearly uniform distribution of the neutral beam and can be made small compared to the plasma cross-section. The region b) consists of closed and nested magnetic surfaces where plasma diffusion can be studied unaffected by the presence of the emitter except for its support. In region c) a limiter or a particle detector can be used in a meaningful manner.

The plasma behaviour in these three regions is governed by

We could not perform new experiments in 1967 as the whole experimental group as well as all the equipment have been moved from the Max-Planck-Institut für Physik und Astrophysik to the Institut für Plasmaphysik.

different laws but the density and its derivative must be adjusted to be equal on either side of the boundaries. The experiments to which the calculations of this report shall be applied have been performed in the stellarator W Ib and have already been described [1, 2].

Fig. 2 gives a scheme of the experiment. The stellarator W Ib has a race track shape. The vacuum tube has a minor diameter of 5 cm, the radius of curvature of the U-bends is 35 cm. The main magnetic field was usually 11 kΓ, the rotational transform produced by a helical field of the type $l = 2$ typically of the order 0.3 Π. The currents producing the magnetic field were switched on for ~ 0.8 sec, a time long enough, as shown later, to reach steady state conditions as far as they can be reached at all with this present set-up. The rise times of the helical field, which was switched on about 0.1 sec after the main field, is short compared with the build-up time of the plasma, but a disturbance of the plasma build-up induced by the rising magnetic field itself cannot be excluded. The plasma was produced by contact ionization on a small tantalum emitter sphere 0.5 cm in diameter, hanging from a 25 μm wire and heated by electron bombardment. The electron beam was switched off about 0.3 sec before the magnetic field was rising. During the course of the actual experiment the temperature of the sphere decreased by 5 to 20 % depending on its initial temperature. The input flux of Cs-ions produced on the sphere was measured and compared with the ion density determined from two single probes located at different distances from the source. Reliable measurements with the very small single probes could only be done if they were placed in the volume defined by these magnetic lines who pass through the sphere (source volume) as only there the single probes did not build up any electric field perpendicular to the magnetic field.

The following model for the calculations takes into account these experimental facts as far as possible.

Throughout the calculations rotational symmetry is assumed, in particular, the magnetic surfaces are thought to have circular cross sections. In the first part of this report inertia terms are neglected

completely. In a second approach, discussed further below, the effect of the inertia will be taken into account in a rather crude manner.

Inside the source volume the density is only slowly varying with r and will therefore be assumed to be constant. Then the individual fluxes have to satisfy the following equation

$$\Phi_o = \Phi_D + \Phi_{Re} + \Phi_s \qquad (1)$$

where

Φ_o : input flux,

Φ_D : flux which is available for building up the density and its distribution; in the steady state it is equal to the flux Φ_{re} which diffuses out of the source volume.

Φ_{Re}: ion flux recombining on the emitter.
$= F(U_{th}(t_o,t))n_o^2$

Φ_s : flux recombining on the probes
$= 2\sqrt{\pi}\ A_s v_{ith} c_s n_o$

A_s = Area of the probes
v_{ith} = most probable velocity of the ions
c_s = correction factor

In our measurements the probes (0.5 cm in length, 50 µm in diameter) have been used only inside the source volume. They measured the density averaged over the source volume if properly adjusted. The input flux, Φ_o, is kept constant. During the density build-up time all other fluxes are time dependent. Φ_{Re} depends strongly on the emitter temperature, and in turn the emitter temperature on time as the heating system is switched off before the experiment starts (fig. 3).

The function $F(U_{th}(U_{th_o},t))$ is given by

$$F(U_{th}(U_{th_o},t)) = 2\pi r_o^2 \frac{e^{-\frac{0.21}{U_{th}(t)}}}{1 + 2e^{-\frac{0.21}{U_{th}(t)}}} \frac{1.11 \cdot 10^{12} e^{\frac{4.1}{U_{th}(t)}}}{3.12 \cdot 10^{28} U_{th}(t)}$$

where

$$U_{th}(t) = U_{th_o} \frac{1}{(1 + 3.63 \frac{3 \cdot 1.03 \cdot 10^5}{r \cdot 3.54 \cdot 10^4} U_{tho} 3.8_t)^{\frac{1}{3.8}}}$$

and the time dependence of the particle density inside the source volume by

$$\dot{n}_o V = \dot{N} = \Phi_D - \Phi_{re} \qquad (2)$$

where N is the total number of particles in the source volume, n_o the density in the source volume and $V = \Pi r_o^2 \cdot L$ the source volume itself.

$r_o = 0.25$ cm is the radius of the emitting sphere, L = 319 cm is the length of the machine and Φ_{re} the flux which diffuses out of the source volume. With the help of eq.(1) we get

$$\dot{n}_o = \frac{1}{V}[\Phi_o - \Phi_{Re} - \Phi_s - \Phi_{re}] \qquad (3)$$

This equation is valid within region a). The flux Φ_{re} entering the region b) is determined by the boundary conditions of region b),

$n(r_o) = n_o$

and

$$\Phi_{re} = -2\Pi \; r \; L \; D(n) \nabla n \text{ for } r = r_o. \qquad (4)$$

In region b) i.e. $0.25 < r < 1.5$ the equation of continuity has the form

$$\dot{n} - \nabla \cdot (D(n) \nabla n) = - (\alpha_1 + \alpha_2 + \alpha_3) n \qquad (5)$$

where

$$D(n) = 2 \eta_\perp \frac{eU_{th_o}}{B^2} \; n(1 + \frac{4\Pi^2}{\iota^2}) \qquad (6)$$

the classical diffusion coefficient modified for stellarator geometry. The different α appearing in eq.(5) represent the coefficients for recombination losses on the surfaces of various obstacles inside the plasma volume or losses to the wall, or in detail $n \alpha_1$ is the flux to the probe supports, $n \alpha_2$ the one to the ring detector, and $n \alpha_3$ the one to the wall of the machine.

This system of two differential equations, eqs.(3) and (5), has been solved numerically.
Before we compare the results with our measurements, we shall discuss the different quantities entering this computation and the correction we have to use compared to our previous evaluations.

Measurements and correction factors

a) Input flux Φ_o

The input ion flux Φ_o could be measured in the presence of the magnetic field by the ion flux to two retractable spoon probes located on the magnetic axis on either side of the emitter. But usually a somewhat different flux Φ_o' was used which was measured by the flux to the wall of the vacuum chamber in the absence of the magnetic field. This flux Φ_o' is reduced by the magnetic field by a factor 0.6 ... 0.8. Unfortunately, this reduction is not known more accurately, and seems slightly to depend on temperature and density. In this evaluation of the measurements, therefore, the input flux is set to $\Phi_o = 0.6 - 0.8\ \Phi_o'$.

The density n_o

The peak density n_o inside the source volume has been measured by two cylindrical probes, both 0.005 cm in diameter and 0.5 cm in length. Earlier we interpreted the probe measurements in the conventionally used Langmuir extrapolation. In the meantime Hashmi et.al.[5] besides other probes calibrated just the probe used in our experiments and compared the probe reading with density measurements by spectroscopic and microwave diagnostic in a Ba plasma. It turned out that the density evaluated from the probe current in the manner used by us would read the density too high by a factor two or three depending on the comparison with the spectroscopic or with the microwave method respectively. We have chosen a factor of 2.5 for the evaluation of our measurements.

The comparison has been made in a single ended Q-machine, so that still some reserve has to be made concerning the density calibration. On the other hand, the factor 2.5 has a theoretically based confirmation by the probe theory of LaFramboise [6].

c) Flux to the ring detector Φ_R

The ring detector is a limiter of 3 cm inner and 4 cm outer diameter screened by a grid of ~ 50 % transparency which is on floating potential. It allows to measure the flux diffusing outwards and reaching the volume defined by the sensitive area of the ring detector which is the case for $1.5 < r < 2$ cm. There is some uncertainty on the efficiency of the detector, but it seems to be near to 1. During the review of the old experiments it turned out that at peak densities higher than $\sim 3 \cdot 10^9$ cm^{-3} the flux to the ring detector starts to grow only proportional to the square root of the input flux, that means proportional to n_o. An explanation of this observation would be that above this density an additional ion flux is leaving the volume defined by the particle detector being proportional to n_o^2. But the density in this region as calculated from the flux found on the particle detector failed by orders of magnitude if these extra losses should be caused by collisional diffusion. It should be mentioned, however, that in the region c) the particle detector is eventually interrupting the secondary currents (if they are not short-circuited across its grids) but it prevents the balancing mass flows parallel to B which are necessary for equilibrium. Therefore the loss rates perpendicular to B must be larger in region c) than in region b). This effect is difficult to treat and has been estimated to be approximated if the diffusion coefficient is enlarged by a factor of 20.
An additional argument yielding an increase of the loss rates from region c) arises from the measurements of the magnetic surfaces by means of an electron beam [3].

There it turned out that the magnetic surfaces in the straight section are still of elliptical cross sections. Especially on this side of the machine where the ring detector was located the ellipse has a ratio of the two axes of 1.5. In addition, the ellipses have found not to be concentric with the ring detector but are displaced by about 0.3 cm. Both these facts mean that only a small part of a magnetic surface is intersecting the ring detector so that on the average a particle has to travel several machine lengths before it hits the ring detector. This enlargement of the effective machine length caused the density in the ring detector volume to grow and, consequently, the losses perpendicular to the magnetic field to gain in importance compared to the losses parallel to the field towards the ring detector. Naturally, also the density calculated from the flux to the ring detector grows if its effective area is smaller than the complete geometric one. In the calculations this effect is taken into account by the "ellipse correction factor" C_E, which is the ratio between the length of ellipse intersecting the ring detector to the circumference of the ellipse.
The shift of the center of the ellipse relative to the center of the ring detector is taken into account by the parameter Δ which is just the distance between these two centres. With this consideration in mind α_2 is

$$\alpha_2 = \frac{v_i}{\sqrt{\pi}L} C_E(\Delta) \tag{7}$$

The flux to the ring detector is then calculated by

$$\Phi_R = 2\sqrt{\pi}\, v_i \int_0^{2.5} r\, n(r, t) C_E(\rho, \eta, \Delta, r) dr \tag{8}$$

with η being the ratio of the axes of the ellipses and $\rho = \sqrt{a \cdot b}$ the mean radius of the ellipse. The choice of the factor 20 mentioned above, enlarging the diffusion in the r.d.volume, the ellipse parameter C_E and the shift parameter Δ have only a minor effect on the peak density n_o.

The aperture

In the earlier evaluation an aperture was taken which was equal to the circular opening of the ring collector. Now the aperture is changed by the elliptical cross section of the magnetic surfaces and by the above mentioned fact, that the density does not yet vanish inside the volume defined by the ring detector. The latter effect is taken into account by a recombination coefficient α_2 being different from 0 (see eq.(7)). $\alpha_3 = 0$ for all magnetic surfaces not intersecting the wall and is put to infinity for those surfaces which do intersect the wall. The effect of the elliptic structure of the magnetic surfaces is further considered by taking the effective cross sections of the magnetic surfaces as circles having the same cross section as the ellipse.

$$\rho = \sqrt{ab} \tag{9}$$

The losses to the probes and to their supports

The fluxes to the probes are

$$\Phi_s = \frac{1}{2\sqrt{\pi}} A_s n_o v_{ith} C_s \qquad \text{with } A_s = 2.78 \cdot 10^{-3} \text{ cm}^2, \tag{10}$$

$$v_i = 1.36 \cdot 10^6 \sqrt{\frac{U_{th}}{A}},$$

$$A = 133 \text{ and}$$

U_{tho} the emitter temperature [eV]

where

A_s is the probe area and C_s the correction factor of 2.5. The correction factor C_s is the same one which is applied to the probe evaluations.

The losses to the probe shafts, which are isolated and therefore on floating potential have also to be corrected for an enlarged ion current. According to LaFramboise [6] this factor at floating potential is about 2.3. The supports are thought to be smeared out over the magnetic surfaces.

Therefore, we get

$$\alpha_2 = \frac{v_i \, r_s}{2\sqrt{\pi} \, r \, L} \cdot C_{s2}$$

$R_s = 7.0 \cdot 10^{-3}$ cm being the radius of the support, $C_{s2} = 2.3$ the correction factor just mentioned.

The rotational transform

The measurements with an electron beam yielded values of the rotational transform being smaller by a factor of 0.875 as assumed earlier [3]. The earlier calculations of this quantity took into account also the effect of the circularizers. As these are not working as perfectly as they should - as shown by the elliptical structure also in the straight sections - it is understandable that also their effect on the rotational transform is smaller than assumed.

The small variation of the rotational transform with the radius is not taken into account, but its value for r = 1.5 cm is taken for the whole range of interest.

The temperature

The temperature has been measured by a two colour pyrometer under steady state operation of the heating system. A relative measurement calibrated against the pyrometer reading is represented by the electron saturation current drawn from the sphere to the wall. An evaluation of the plasma results has shown, that they could be explained only if the temperature were higher by about 140 ^{o}K than stated earlier. This result arose from the sharp decrease of the density and the flux to the ring detector if the temperature is lowered and the recombination flux therefore increased.

A check of our pyrometer showed, that it was reading the temperature too low requiring a correction of about 100 ^{o} - 200 ^{o}K depending on temperature. The initial temperatures used in the calculations

are the temperatures at the time the helical field is switched on, whereas the temperatures stated in the experiments are the temperatures at the time the electron beam is switched off, which is 0.3 sec earlier.

Comparison of the experimental results with the numerical calculations

On the basis of the model mentioned above numerical calculations have been performed which deviate from the earlier calculations by the points summarized again:

a) The flux to the probes is increased by the same factor, which reduces the density in the experimental results.
b) The shafts of the probes have been taken into account, using an appropriate correction factor for the flux.
c) The flux to the ring detector and the aperture is changed by the elliptical cross section of the magnetic surfaces.
d) The loss of equilibrium in the volume defined by the ring detector is approximated by an increased diffusion.
e) The variation of the emitter temperature with time is taken into account.

The evaluation of the experimental results has been corrected according to the new results:

a) A factor of 2.5 has been applied in evaluating the density n_o.
b) The input flux $\Phi_o = 0.6 - 0.8\ \Phi_o^{\uparrow}$ is used for comparison instead of the ring detector flux Φ_R.
c) The magnitude of the rotational transform is changed according to the electron beam measurements ($_{new} = 0.875$ old).
d) The correct value of the emitter temperature is used.

Figs. 4a and b show the time dependence of all densities and fluxes calculated for input fluxes of $1 \cdot 10^{12}$ and $1 \cdot 10^{14}$ resp. Fig. 5 shows the time dependence of the density n_o in the source volume with the input flux as parameter for an emitter temperature of $U_{tho} = 0.18$ eV at t = 0.It is to be seen that due to the decrease of the temperature with time the peak density is decreasing already very early, so that a real stationary state can never be established. Fig. 6 shows the

same dependence for different values of U_{tho}. Fig. 7 is a comparison between the experimental probe signal (mean value of both probes) and the calculated density for two different input fluxes, $\Phi = 1 \cdot 10^{12}$ sec^{-1} and $3 \cdot 10^{12}$ sec^{-1}. In the experiment Φ_o was $1.7 \cdot 10^{12}$ sec^{-1} and $2.2 \cdot 10^{12}$ sec^{-1} respectively. The bars show the calculated peak density for $U_{tho} = 0.18$ and 0.2 eV and $\Phi_o = 0.6 - 0.8\ \Phi_o'$. Figs. 8 and 9 give the same comparison for $\Phi_o \sim 1 \cdot 10^{13}$ sec^{-1} and $\sim 1 \cdot 10^{14}$ sec^{-1} respectively. It is clearly seen that for input ion fluxes of 10^{12} sec^{-1} the experimental result is closely reproduced by the calculations in both respects, peak ion density achieved and time dependence of the density. For input ion fluxes above 10^{13} sec^{-1}, however, the observed rise of the ion density is suddenly interrupted at about 75 % of the calculated final density yielding a too low peak density and simulating a too small rise time (defined as the time necessary to reach 80 % of the peak density). This behaviour is shown in fig.10 where, as a function of the input ion flux, the measured peak ion densities are compared with the theoretical curves. For fluxes above 10^{13} sec^{-1} a deviation from the calculated peak densities is observed, whereas below 10^{13} sec^{-1} the agreement with the calculations is quite good. Fig. 11 shows the same experimental results being compared with a set of curves calculated for different diffusion coefficients as parameter. The diffusion coefficients are given as multiples of the resistive diffusion coefficient varied for stellarator condition. From this point of view a diffusion coefficient of up to two times that for resistive diffusion would still fit the experimental values. The rise time of the ion density as defined above versus the input ion flux is plotted in fig. 12. As already mentioned it shows agreement with the calculations at lower input fluxes but at higher fluxes quite large deviations are observed (compare figs. 8 - 10). At the highest fluxes the rise time was not measured exactly enough as the experiment has not been laid out for the observation of the instationary state.

For a stellarator the classical diffusion coefficient has to be modified by a factor $1 + 4(\frac{\Pi}{\iota})^2$ due to the energy dissipation of the

secondary currents. Fig. 13 shows this factor plotted versus Φ_o/n_o^2 which would be a measure of the diffusion coefficient itself. But due to the fluxes recombining on the probes the calculated curves are no straight lines and, in addition, differ for different values of the input flux. But the agreement at medium values of L is quite good and also the general trend of the curve is found as expected. The deviations at low values of L shall be considered later.

Worse than the other ones is the comparison between the calculated and observed flux to the ring detector (fig. 14). According to the calculations the flux to the ring detector should appear not earlier than a few hundred milliseconds after the rise of the magnetic field (see fig. 4), whereas the observed flux is starting nearly immediately. If one neglects the non-appearance of this time delay one must state that the rise time observed is not too far from the calculated one. In addition, the absolute values of the peak ion flux found on the particle detector which, according to the calculations, for low input fluxes should be reached only after a few seconds, is in rough agreement with the calculations but somewhat too small at higher input fluxes and somewhat too large at lower input fluxes.

Unfortunately, the influence of the presence of probes within the plasma on peak ion density and flux found on the ring detector was measured only for an input ion flux of $1 \cdot 10^{12}$ sec^{-1}. The results obtained only roughly agree with the calculations but fit with the other observations concerning the particle detector.

In summarizing, the only considerable deviations between experimental and theoretical results observed are the following ones

1) the peak ion density for input ion fluxes above 10^{13} sec^{-1},
2) the rise time of the peak ion density for input ion fluxes above 10^{13} sec^{-1} although this effect is clearly connected with 1), the interruption of the further build-up of the central density,
3) the missing of the time delay of the rise of the flux to the ring detector
4) the relation between the input flux and the flux to the ring detector.

As point 4) is concerned, it is certainly wrong to compare the experimental results obtained 0.8 sec after switching on the magnetic field with the calculated fluxes obtained for about 3 sec after the start of the experiment. At this time the emitter has cooled down already so much that a large fraction of the input flux is lost again on its surface which otherwise would be lost by diffusion. In estimating this effect, one should expect indeed a somewhat larger flux moving to the ring detector as indicated by the dashed line shown in fig. 14. Furthermore, in this range the calculated flux to the ring detector depends sensitively on Δ, the displacement between the center of the cross section of the magnetic surfaces and the one of the ring detector. Therefore, at least for smaller input ion fluxes, there is no serious deviation between the measured and the calculated results. At higher input fluxes even an enlargement of the resistive diffusion coefficient by a factor of 300 inside the volume defined by the ring detector volume gives not as large a reduction of the signal as observed. Calculations taking into account loss of equilibrium rather than enlarged diffusion are under way; they should yield a better accordance with the measurements. As far as the points 1) - 3) are concerned these deviations from the model assumed might be caused by a partial lack of equilibrium either in time - that means preferentially during the rise time - or in space, particularly in regions with steep density gradients. According to the Pfirsch-Schlüter model equilibrium between plasma pressure and magnetic field forces requires the existence of a mass flow parallel to the magnetic lines. As the only force available to drive this mass motion is a pressure gradient parallel to B equilibrium should be lost at the latest if the required velocity exceeds the thermal velocity of the ions. Eckhartt and Grieger [7] have given the following inequality for this limit

$$- 1.94 \cdot 10^{-27} \frac{\pi^3}{l^3} \frac{\sqrt{A} \cdot \ln\Lambda}{B_o^2 U_{th}} \frac{R_o L}{2\pi r^2} \nabla n \ll 1 \qquad (11)$$

where A is the atomic mass number of the ions, R_o the radius of

curvature and L the length of the machine. Compared to the inequality given in ref.[7] R_o^2 has been replaced by $\frac{R_o L}{2\pi}$ in order to take into account also the straight sections of the device.This condition is valid in this form if the perpendicular component of the ion pressure gradient is balanced by an electric field and the diamagnetic current is carried by the electrons which fits the usual assumptions. For the conditions of the experiments done in the stellarator W Ib the above inequality reduces to

$$-\frac{\nabla n}{r^2}\left(\frac{\pi}{\iota}\right)^3 \ll 5.2\cdot 10^{11}\ [\mathrm{cm}^{-6}] \text{ for } U_{th} = 0.18\ \mathrm{V} \qquad (12)$$

$$\ll 5.8\cdot 10^{11}\ [\mathrm{cm}^{-6}] \text{ for } U_{th} = 0.20\ \mathrm{V}$$

For an input ion flux of 10^{12} sec^{-1} fig. 15a shows a profile of particle density as it develops with time, and fig. 16 the stationary profile for different values of the input flux. In figs. 15b and 16b the quantity $-\frac{\nabla n}{r^2}\left(\frac{\pi}{\iota}\right)^3$ vs. r is plotted. One sees that the limit set by (12) for low input fluxes is slightly surpassed during the build-up phase and just reaches the limit in the final state. For higher input fluxes, however, the limit is largely exceeded also in the final state. To this picture fits the experimental observation that, preferentially at high input fluxes,the build-up of the peak density shows sudden stops and even decreases whereas at the same time the ring detector flux shows large bursts (see fig. 17). This might be explained, therefore, by a sudden loss of equilibrium by which effect plasma is swept across the confinement region to the ring detector. A more refined model must take into account the effect of the ion inertia which is a very difficult task to do. However, if one restricts oneself to a description of the gross behaviour only one might find rough agreement with the experimental observations upon requiring that the density gradient should not exceed the limit set by the inequality (12)

$$\nabla n \leq 5.2\cdot 10^{11}\ r^2\left(\frac{\iota}{\pi}\right)^3 \cdot \alpha \qquad (13)$$

where α, $0 < \alpha < 1$, is the ratio between the "cut-off" velocity and the thermal velocity of the ions. If this would become the case the local diffusion coefficient is increased until eq.(13) is satisfied. This procedure happens to become necessary for radii smaller than a critical radius, r_{cr}. For $r \leq r_{cr}$ the profile of particle density is then obtained by integrating eq.(13) with respect to r

$$n = 1.73 \cdot 10^{11} \left(\frac{\iota}{\pi}\right)^3 \alpha (r_{cr}^3 - r^3) + n_{cr} \qquad (14)$$

n_{cr} being the density for $r = r_{cr}$. This equation yields new values for the peak ion density to be compared with the experimental results shown in figs. 10 and 11. These values vs. Φ_o are plotted in fig. 18 for three different values of α, $\alpha = 1$; 2, and 3, depending on whether the "cut-off" velocity is 1, 2, or 3 times the ion thermal velocity. The earlier calculations, the results of which are shown for comparison, have neglected ion inertia completely which corresponds to $\alpha \to \infty$. In fig. 19 the same correction is applied to the dependence of the peak ion density on ι as it was shown in fig. 13. With these corrections rather close agreement is obtained with the experimental results.
It is believed that a more realistic but thus more complicated model would explain also the early rise of signal found on the particle detector. In this respect it should be an essential point that there is already some plasma in the machine and some signal detected on the particle detector if only the main magnetic field is present and the helical field is not yet switched on.
In addition it should be noted that some problems connected with the thermalization of the plasma should arise at low values of the input flux. This effect has not been considered in this report but has already been mentioned in refs.[2] and [3].

Conclusions

Taking into account all corrections listed in this report most of the experimental facts found for a Cs plasma in the stellarator W Ib are reproduced within a factor of 2 by calculations based upon a model which assumes resistive diffusion across the stellarator magnetic field and recombination on the surfaces of the emitter and the probes. Larger deviations from this model are found to be caused by an influence of ion inertia on the equilibrium properties. Estimations of this effect yield fair agreement with the experimental observations also for these cases. Equilibrium seems to be lost if the required velocity of the balancing mass flow exceeds the ion thermal velocity by a factor between 1 and 2.

The numerical scheme

The set of equations (4), (5), (6) can, after suitable scaling, be written in dimensionless form:

$$\dot{n}_o = 1 - F\, n_o^2 - S\, n_o + \gamma \frac{\partial n_o^2}{\partial r}, \qquad r = 1 \tag{15}$$

$$\dot{n} = \frac{1}{r}\frac{\partial}{\partial r}\left(r\gamma n \frac{\partial n}{\partial r}\right) - \sum_{j=1}^{3} {}^{(j)}\alpha\, n, \qquad r > 1 \tag{16}$$

where F is the (time dependent) factor of the recombination flux, S represents the flux to the probes and the ${}^{(j)}\alpha$ give the fluxes to the probe support, to the detector and to the wall respectively. They are time- and space dependent, for details cf. eqs.(1) resp. (7) and (8). The dimensionless radius of the source volume is set equal to one and the diffusion coefficient is represented by

$$D(n) = \gamma n \tag{17}$$

(cf. eq.(6)).

For discretisation, we chose the points

$$r_i = 1 + (i - \tfrac{1}{2})\Delta r, \qquad i = 0, 1, \ldots N \tag{18}$$

i.e. the source radius $r_o = 1$ is situated midways between two meshpoints to allow a simple second order approximation to the derivative in eq.(15). The outermost point r_N corresponds to the outer wall where n is set equal to zero. Because of the nonlinearity, a simple explicit scheme was adopted:

$$\text{Let} \quad n_i = n(r_i, t); \qquad \overset{+}{n}_i = n(r_i, t + \Delta t) \tag{19}$$

The scheme reads

$$\overset{+}{n}_o = n_o + \Delta t\left(1 - Fn_o^2 - Sn_o + \gamma \frac{n_1^2 - n_2^2}{\Delta r}\right) \tag{20}$$

$$\overset{+}{n}_i = n_i + \frac{\Delta t}{\Delta r^2}\frac{1}{2r_i}\left[\gamma_{i+\frac{1}{2}}\, r_{i+\frac{1}{2}}\,(n_{i+1}^2 - n_i^2) - \right.$$

$$\left. - \gamma_{i-\frac{1}{2}}\, r_{i-\frac{1}{2}}\,(n_i^2 - n_{i-1}^2)\right] - \Delta t \sum_j {}^{(j)}\alpha\, n_i \qquad (21)$$

$$\overset{+}{n}_N = n_N = 0 \qquad (22)$$

As the coefficient of diffusion was to be increased by a factor of 20 (or more) within the detector, γ is space- as well as time dependent. For initial condition, $n_i = 0$ for $t = 0$ was chosen. The scheme is conservative, i.e. if we approximate the integrals entering the various fluxes and so on by the trapezoidal rule the change in total particle number per timestep is exactly given by the balance of the various fluxes.

The question of the numerical stability can be handled in the following way: Eq.(21) may be rewritten into

$$\overset{+}{n}_i = A_i n_{i+1} + B_i n_i + C_i n_{i-1} - \Delta t \sum_j {}^{(j)}\alpha\, n_i \qquad (23)$$

with

$$A_i = \frac{\Delta t}{\Delta r^2}\,\frac{\gamma_{i+\frac{1}{2}}\; r_{i+\frac{1}{2}}}{2r_i}\,(n_{i+1} + n_i),$$

$$C_i = A_{i-1}$$

$$B_i = 1 - A_i - A_{i-1},$$

which may be verified by direct substitution. We have

$$A_i + B_i + C_i = 1,$$

and if all 3 quantities are positive or zero, we may estimate

$$\underset{i}{\mathrm{Max}}|\overset{+}{n}_i| \leq \underset{i}{\mathrm{Max}}|n_i|(1 + O(\Delta t)), \tag{24}$$

the solution is bounded for any finite time interval. Now

$$B_i = 1 - \frac{\Delta t}{\Delta r^2}\frac{1}{2}\left[\frac{\gamma_{i+\frac{1}{2}}\, r_{i+\frac{1}{2}}}{r_i}(n_{i+1} + n_i) + \frac{\gamma_{i-\frac{1}{2}} r_{i-\frac{1}{2}}}{r_{i-1}}(n_i + n_{i-1})\right]$$

is the only quantity that may become negative if $n_i \geq 0$, wherefore

$$n_i \geq 0, \quad \Delta t \leq \frac{1}{2}\frac{\Delta r^2}{\underset{i}{\mathrm{Max}}(\gamma_i n_i)} \tag{25}$$

is sufficient for stability, and the first condition is satisfied automatically by virtue of the scheme (21) if it holfs initially, provided the second holds.
If in numerical tests this condition was violated by only a few percent, the numerical solution was completely swamped within a few time cycles, so it is probably necessary as well. For the actual calculation, we chose N = 40 in eq.(18), i.e. 40 meshpoints. Tests with 60 points brought about changes of at most a few percent, so 40 was chosen as a safe compromise between accuracy and computing time.

The smallest timestep became a little awkward after the build-up while computing the slow changes caused by the temperature drop of the emitter.

Here, an implicit scheme would have been advantageous despite the nonlinear character of the equations, which would have forced us to adopt an iterative procedure for its solution.

References

[1] D.Eckhartt, G.v.Gierke, G.Grieger — Plasma Physics and Contr.Nucl.Fusion Res. Vol.II, 719 (1966)

[2] D.Eckhartt, G.v.Gierke, G.Grieger — Institut für Plasmaphysik Report IPP 2/52 (1966)

E.Berkl, D.Eckhartt, G.v.Gierke, G.Grieger — Phys.Rev.Letters 17, 906 (1966)

[3] E.Berkl, G.v.Gierke, G.Grieger — Institut für Plasmaphysik Report IPP 2/69 (1968)

[4] S.v.Goeler — Phys.Fluids 7, 463 (1964)

[5] M.Hashmi, A.J.van der Houven van Oordt, J.-G.Wegrowe — 2nd European Conf.on Contr.Fusion and Plasma Physics, Stockholm 1967 (to be published in Plasma Physics)

[6] J.G.La Framboise — Institute for Aerospace Studies University of Toronto UTIAS Rep.No. 100

[7] D.Eckhartt, G.Grieger — Max-Planck-Institut für Physik und Astrophysik Report MPI-PA-29/64 (1964)

Figure Captions

Fig. 1 Schematic comparison between a linear Q-machine and a "toroidal" one.
Region a is the illuminated part of the emitter; b the region where diffusion is to be observed; c, the region where the density is falling to zero.

Fig. 2 Scheme of the experimental set-up of the stellarator W Ib.

Fig. 3 Temperature of the emitting sphere vs. time for different initial temperatures.

Fig. 4 a) Calculated time dependence of the ion density and the various loss fluxes for an input flux of $\Phi_o = 1 \cdot 10^{12}$ sec^{-1}; B = 11 kΓ, $\iota = 0.26$ Π, $\Delta = 0.3$ cm, two probes present within the plasma;
b) The same for an input flux of $\Phi_o = 1 \cdot 10^{14}$ sec^{-1}.

Fig. 5 Calculated time dependence of the peak density n_o for different input fluxes. B = 11 kΓ, $\iota = 0.26$ Π, $\Delta = 0.3$ cm, two probes.

Fig. 6 Calculated time dependence of the peak density n_o for different input fluxes Φ_o and initial temperatures of the emitter, U_{tho}. The parameters are the same as in fig.5.

Fig. 7 Comparison between experimental probe-signals (mean value of both probes) obtained for two different input fluxes, $\Phi_o' = 1.7 \cdot 10^{12}$ sec^{-1} and $\Phi_o' = 2.2 \cdot 10^{12}$ sec^{-1}, and calculated curves for $\Phi_o = 1 \cdot 10^{12}$ sec^{-1} and $3 \cdot 10^{12}$ sec^{-1}. The bars show the calculated peak densities for Φ_o between 0.6 Φ_o' and 0.8 Φ_o' and for U_{tho} = 0.18 and 0.2 V resp. For the parameters see fig. 5.

Fig. 8 The same as fig. 7 for an experimental input flux $\Phi_o' = 1 \cdot 10^{13}$ sec^{-1} and $3 \cdot 10^{13}$ sec^{-1}.

Fig. 9 The same as fig. 7 but for an experimental input flux Φ_o' $1.86 \cdot 10^{14}$ sec^{-1} and calculated input fluxes $1 \cdot 10^{14}$ sec^{-1} and $3 \cdot 10^{14}$ sec^{-1}.

Fig. 10 Comparison between the experimentally found peak densities vs. input flux Φ_o and the calculated curves for $U_{tho} = 0.18$ and 0.2 V. The bars indicate the range of $\Phi_o = 0.6 - 0.8\ \Phi_o'$. Parameters as in fig. 5.

Fig. 11 The same experimental values as given in fig. 10 being compared with calculated curves for different diffusion coefficients and $U_{th} = 0.18$ and 0.20V parameters as in fig. 5.

Fig. 12 Comparison between the experimental and calculated rise times (80 % of peak value; in the experimental case the signal of the distant probe has been evaluated) vs. Φ_o.
Curve 1: $U_{th} = 0.2$ V, two probes
curve 2: $U_{tho} = 0.2$ V, without probes
curve 3: $U_{tho} = 0.18$ V, two probes.
Parameters as in fig. 5.

Fig. 13 $1 + 4(\frac{\Pi}{l})^2$ vs. $\frac{\Phi_o}{2}$. The bars (8) indicate the range of $\Phi_o = 0.6 - 0.8\ \Phi_o'$, B = 11 kΓ.
Curve 1: $\Phi_o = 3 \cdot 10^{13}$ $U_{tho} = 0.2$ V, without probes
curve 2: $\Phi_o = 1 \cdot 10^{12}$ $U_{tho} = 0.2$ V, without probes
curve 3: $\Phi_o = 3 \cdot 10^{13}$ $U_{tho} = 0.2$ V, two probes
curve 4: $\Phi_o = 1 \cdot 10^{13}$ $U_{tho} = 0.2$ V, two probes
curve 5: $\Phi_o = 1 \cdot 10^{13}$ $U_{tho} = 0.18$V, two probes
curve 6: $\Phi_o = 1 \cdot 10^{12}$ $U_{tho} = 0.2$ V, two probes
curve 7: $\Phi_o = 1 \cdot 10^{12}$ $U_{tho} = 0.18$ V, two probes
The experimental values are taken for an input flux of $\Phi_o' = 2.2 \cdot 10^{12}$ sec^{-1} that is $\Phi_o = 1.3 - 1.75 \cdot 10^{12}$ sec^{-1} and an initial temperature of the emitter sphere of about 0.18 V.

Fig. 14 Peak flux to the ring detector, Φ_{max}, vs. Φ_o. The bars indicate the range $\Phi_o = 0.6 - 0.8\ \Phi_o^*$. The dashed line shows the trend of the calculated curve when correcting for the fact that the calculated peak flux is reached comparatively late. B = 11 kΓ, $\iota = 0.26\ \Pi$, two probes, $\Delta = 0.3$ cm. At lower input fluxes this relation is very sensitive to the magnitude of Δ.

Fig. 15 a) Calculated profiles of ion density for an input flux of $\Phi_o = 1 \cdot 10^{12}$ sec^{-1} at different times (0.2 ... 3 sec).

b) $-\frac{\nabla n}{(\frac{\iota}{\Pi})^3 r^2}$ vs. r for the profiles shown in fig. 15a.

Fig. 16 Profiles of ion density calculated for different input fluxes, Φ_o. The time for which the profiles are shown was chosen as close as possible to the time at which the density was maximum but so that the flux to the ring detector had surpassed already its maximum. B = 11 kΓ, $\iota = 0.26$, two probes, $U_{tho} = 0.18$ V, $\Delta = 0.3$ cm except for the profile with $\Phi_o = 1 \cdot 10^{13}$ sec^{-1} where $\Delta = 0.5$ cm.

Fig. 17 Upper picture: Experimental probe signals;
lower picture: flux to the two sides of the ring detector.

Fig. 18 Peak density n_o vs. Φ_o as shown in fig. 10. Besides the calculated curve for $U_{tho} = 0.18$ V, curves modified by the ∇ n-condition (eq.(14)) are drawn. 1, 2, 3 corresponds to the "cut-off" velocities of the balancing mass flows being 1, 2, 3 times the thermal ion velocity. B = 11 kΓ, $\iota = 0.26\ \Pi$, two probes, $\Delta = 0.3$ cm.

Fig. 19 $1 + 4(\frac{\Pi}{\iota})^2$ vs. Φ_o as shown in fig. 13. Besides the calculated curve for $U_{tho} = 0.18$ V the curves modified by the ∇ n condition (eq.(14)) are drawn. 1, 2, 3 corresponds to the "cut-off" velocities of the balancing mass flows being 1, 2, 3 times the thermal ion velocity. B = 11 kГ, $\iota = 0.26\ \Pi$, two probes, $\Delta = 0.3$ cm.

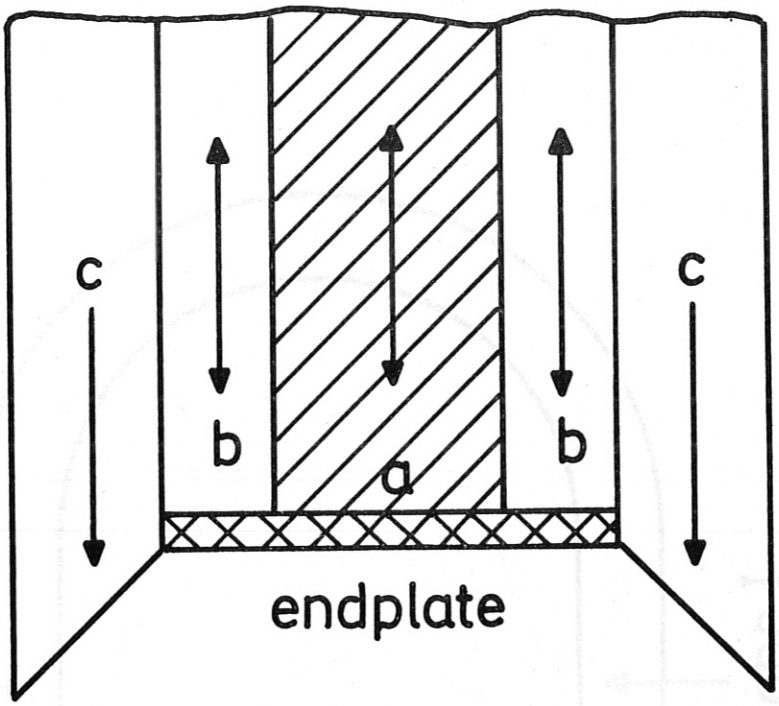

linear Q-machine

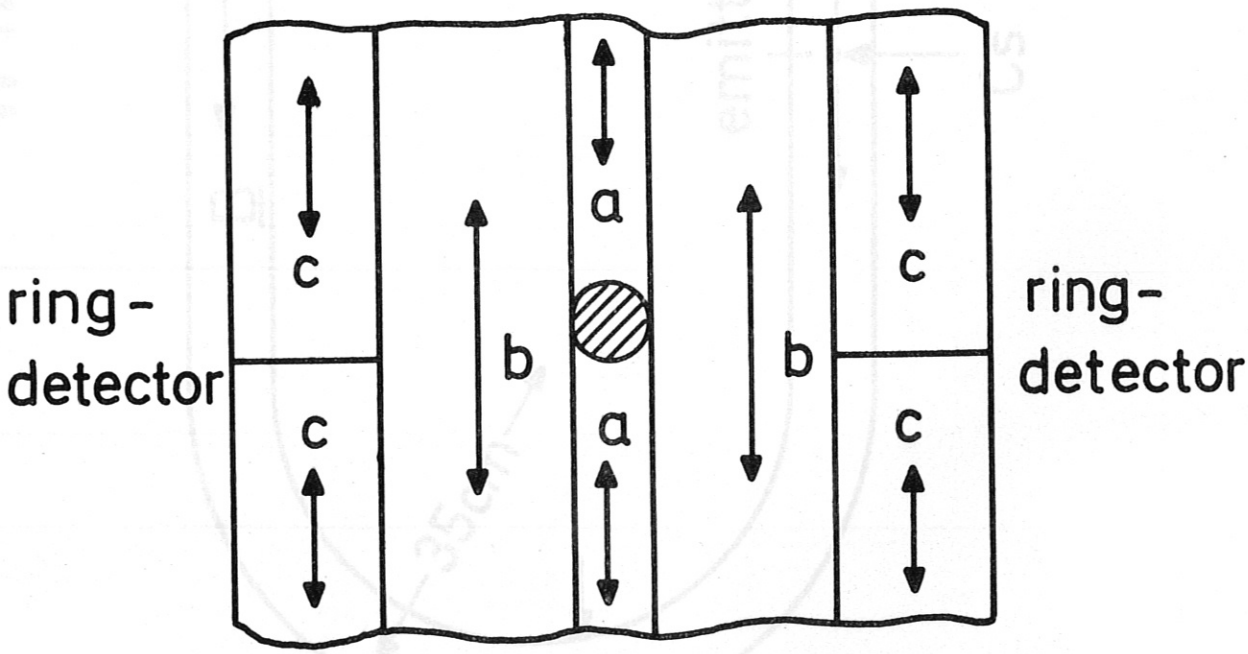

"toroidale" Q-machine

Fig.1

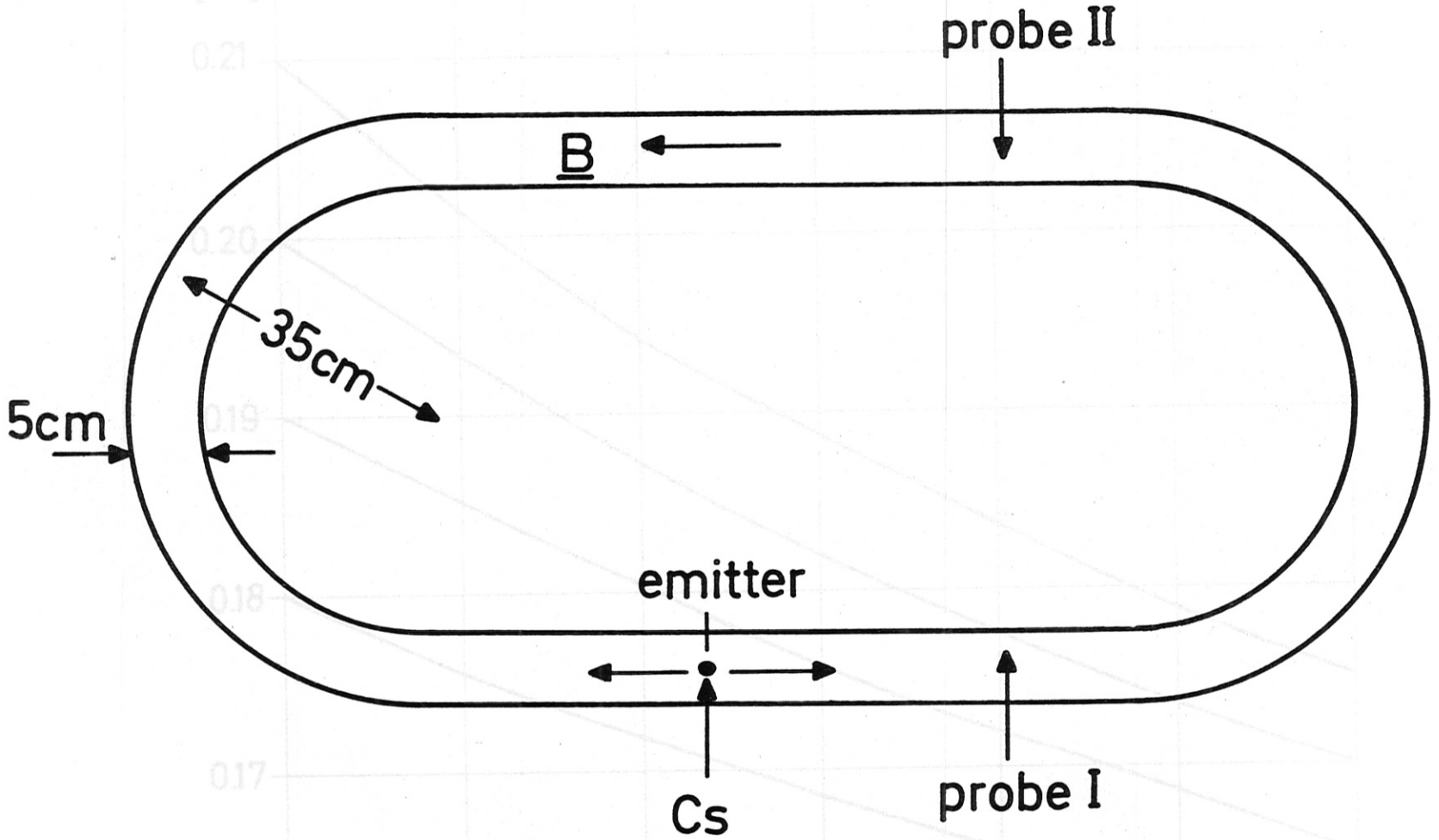

Fig. 2

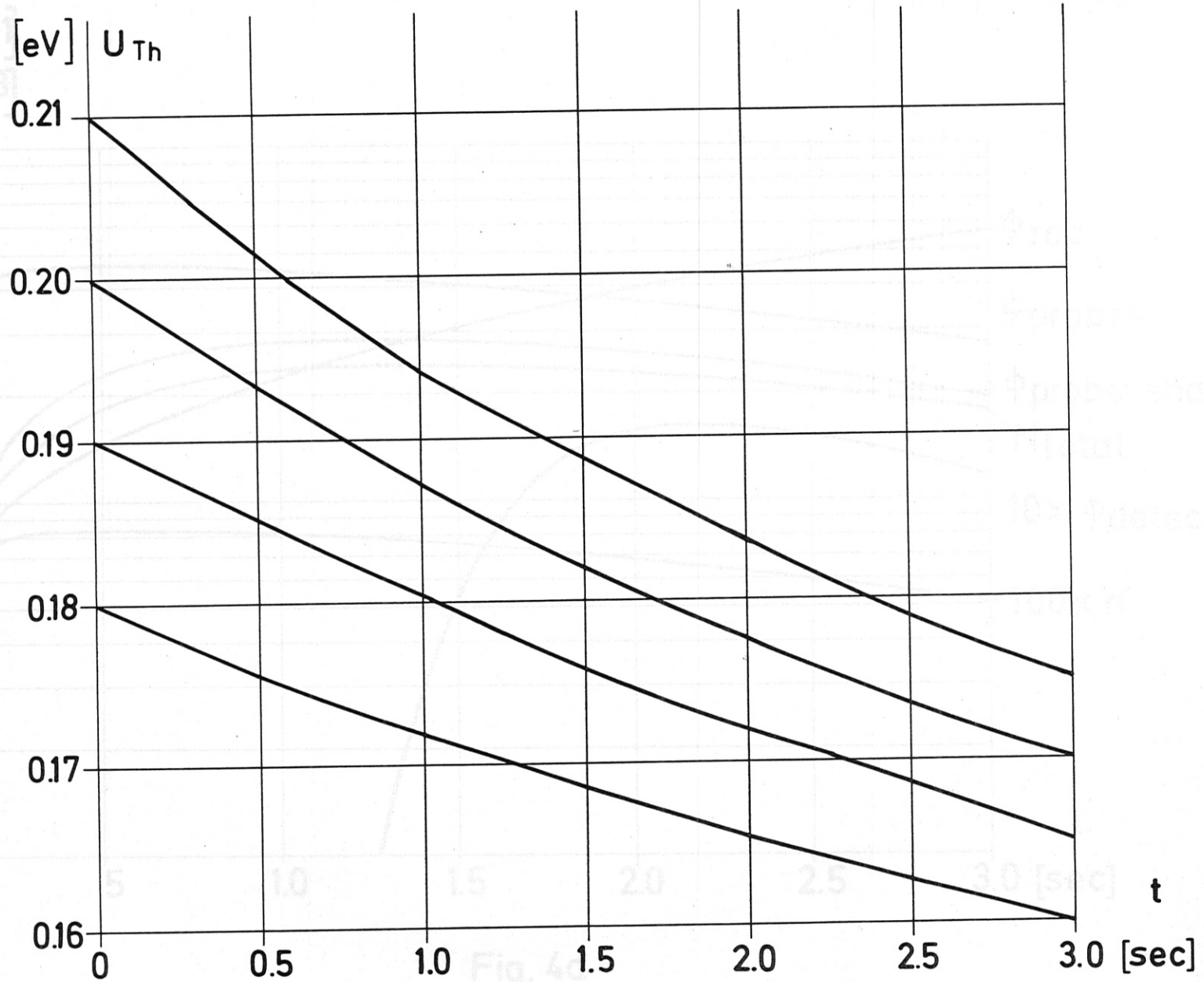

Fig. 3

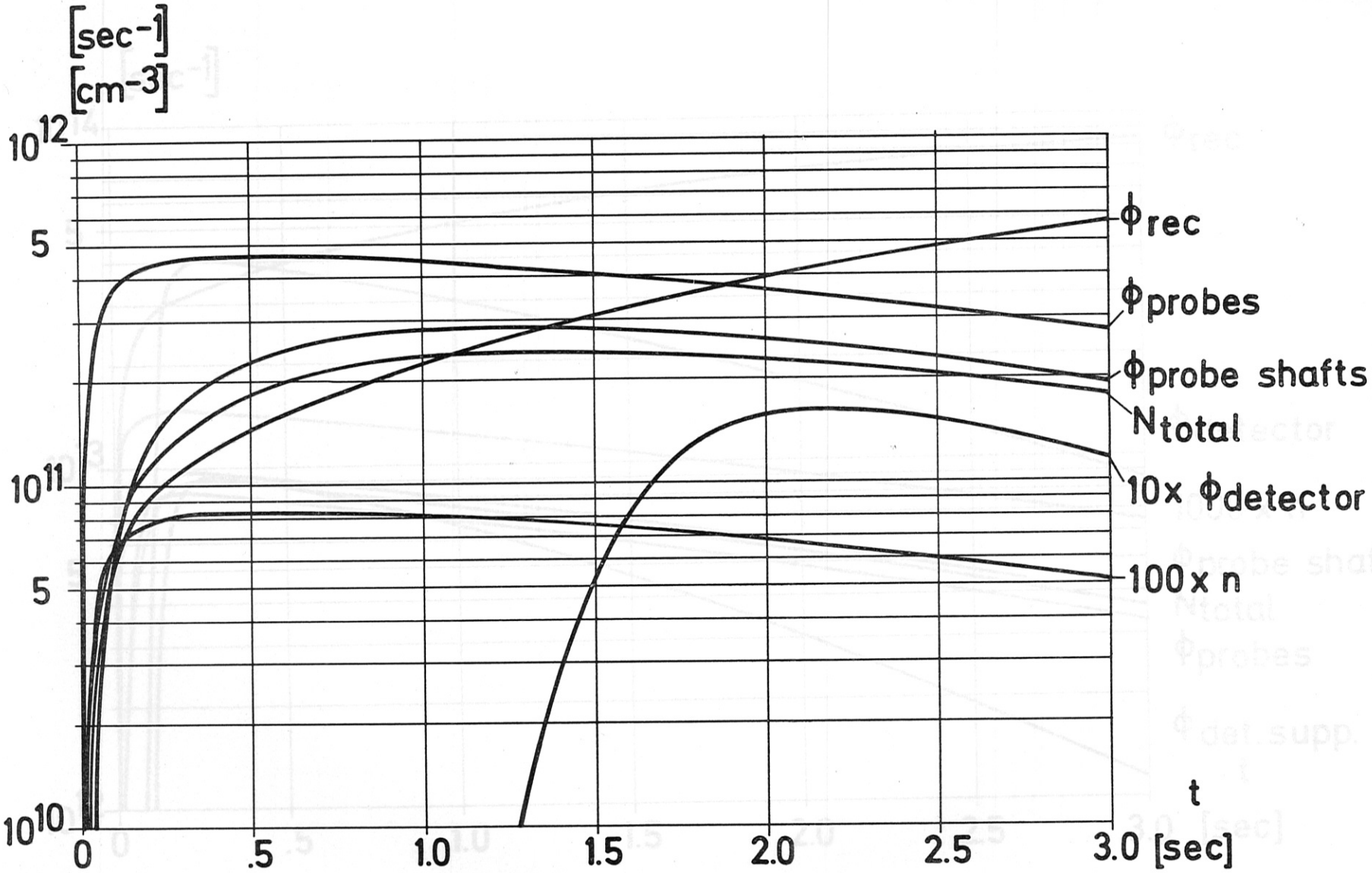
[sec-1]
[cm-3]
10^12
5
10^11
5
10^10
0
.5
1.0
1.5
2.0
2.5
3.0 [sec]
t
φrec
φprobes
φprobe shafts
Ntotal
10x φdetector
100x n

Fig. 4a

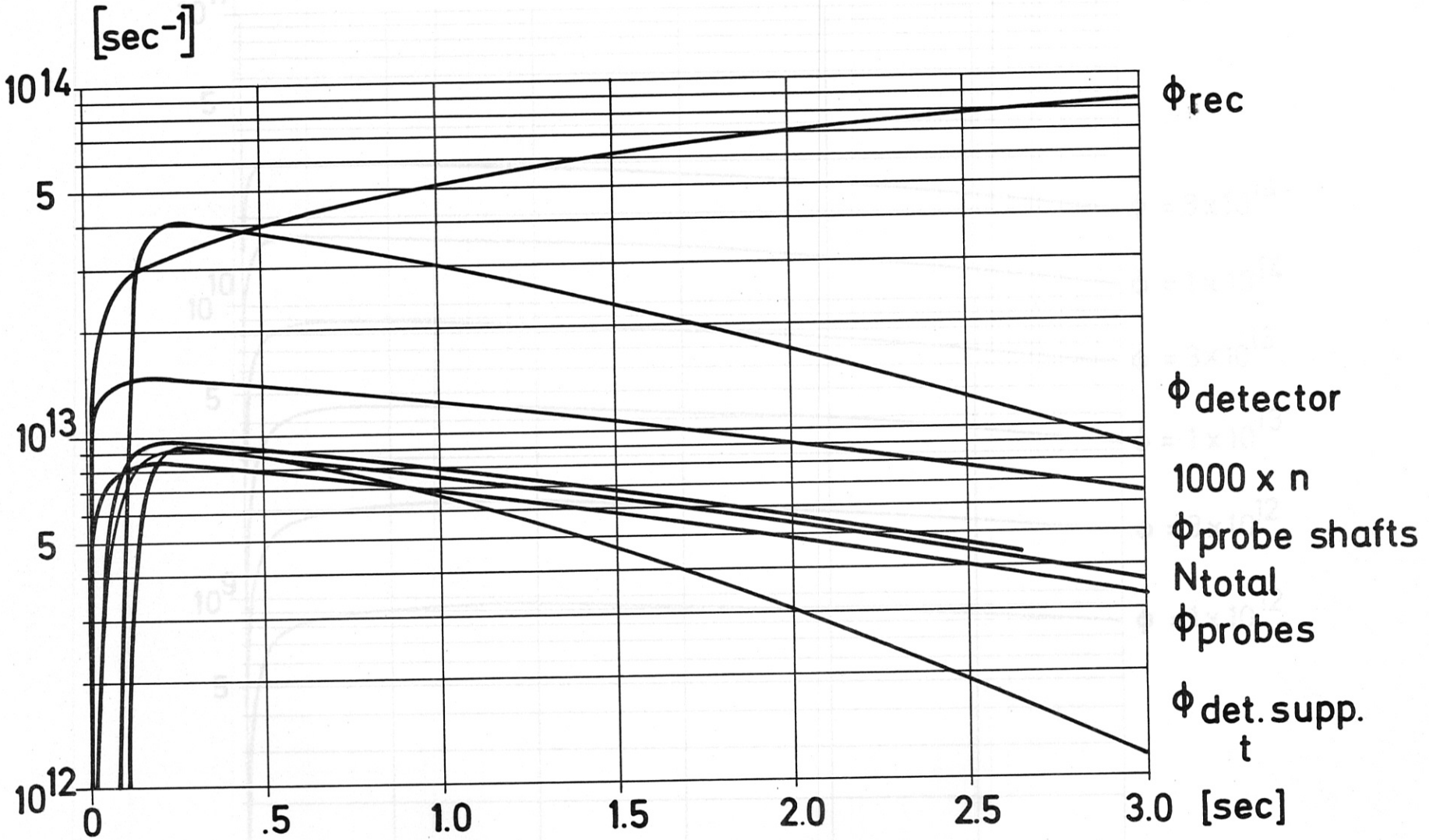
[sec⁻¹]
10¹⁴
5
10¹³
5
10¹²
0
.5
1.0
1.5
2.0
2.5
3.0
[sec]
φrec
φdetector
1000 x n
φprobe shafts
Ntotal
φprobes
φdet. supp.
t

Fig. 4b

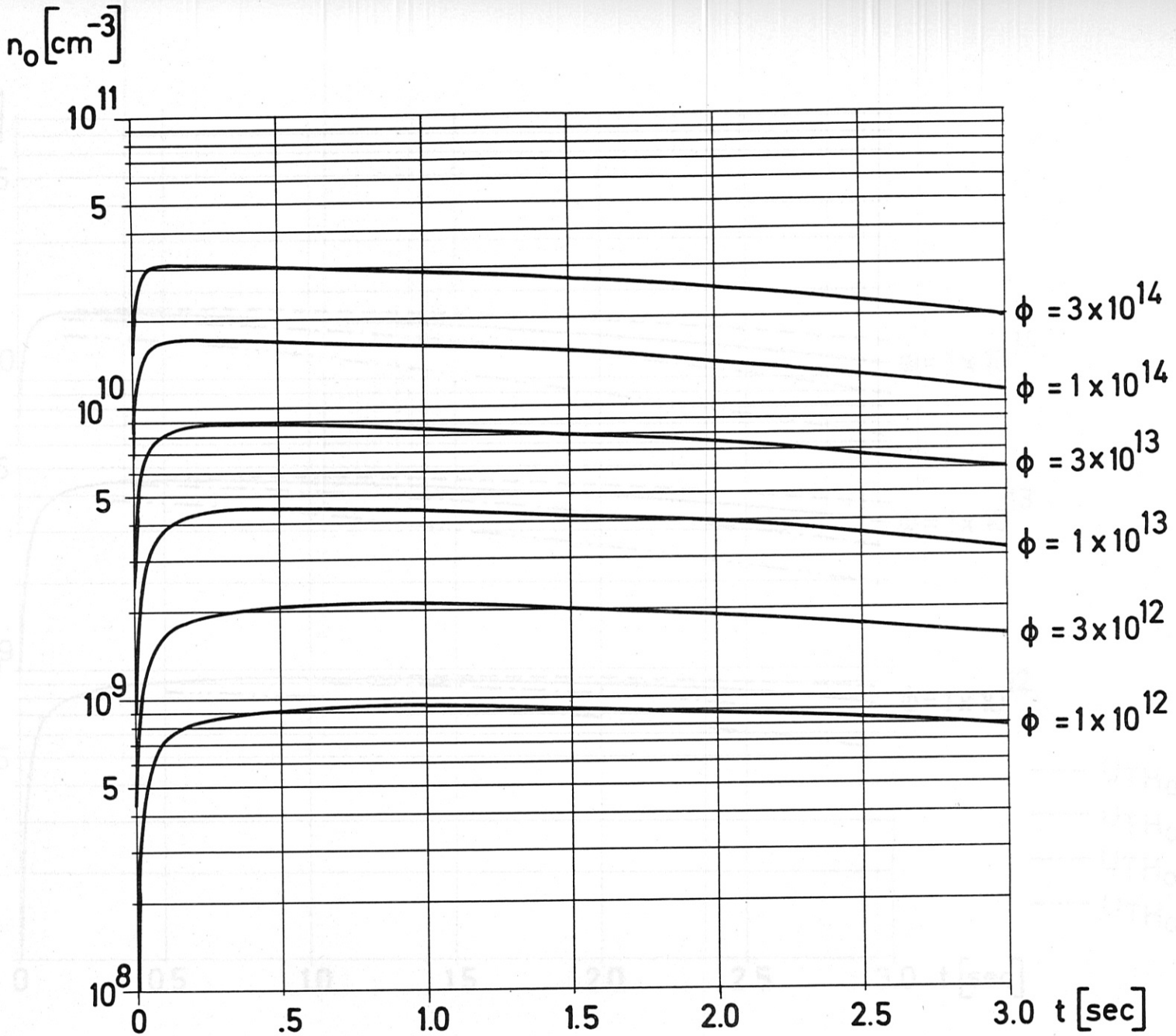
$n_o[cm^{-3}]$
10^{11}
5
10^{10}
5
10^{9}
5
10^{8}
$\phi = 3 \times 10^{14}$
$\phi = 1 \times 10^{14}$
$\phi = 3 \times 10^{13}$
$\phi = 1 \times 10^{13}$
$\phi = 3 \times 10^{12}$
$\phi = 1 \times 10^{12}$
0
.5
1.0
1.5
2.0
2.5
3.0
t [sec]

Fig. 5

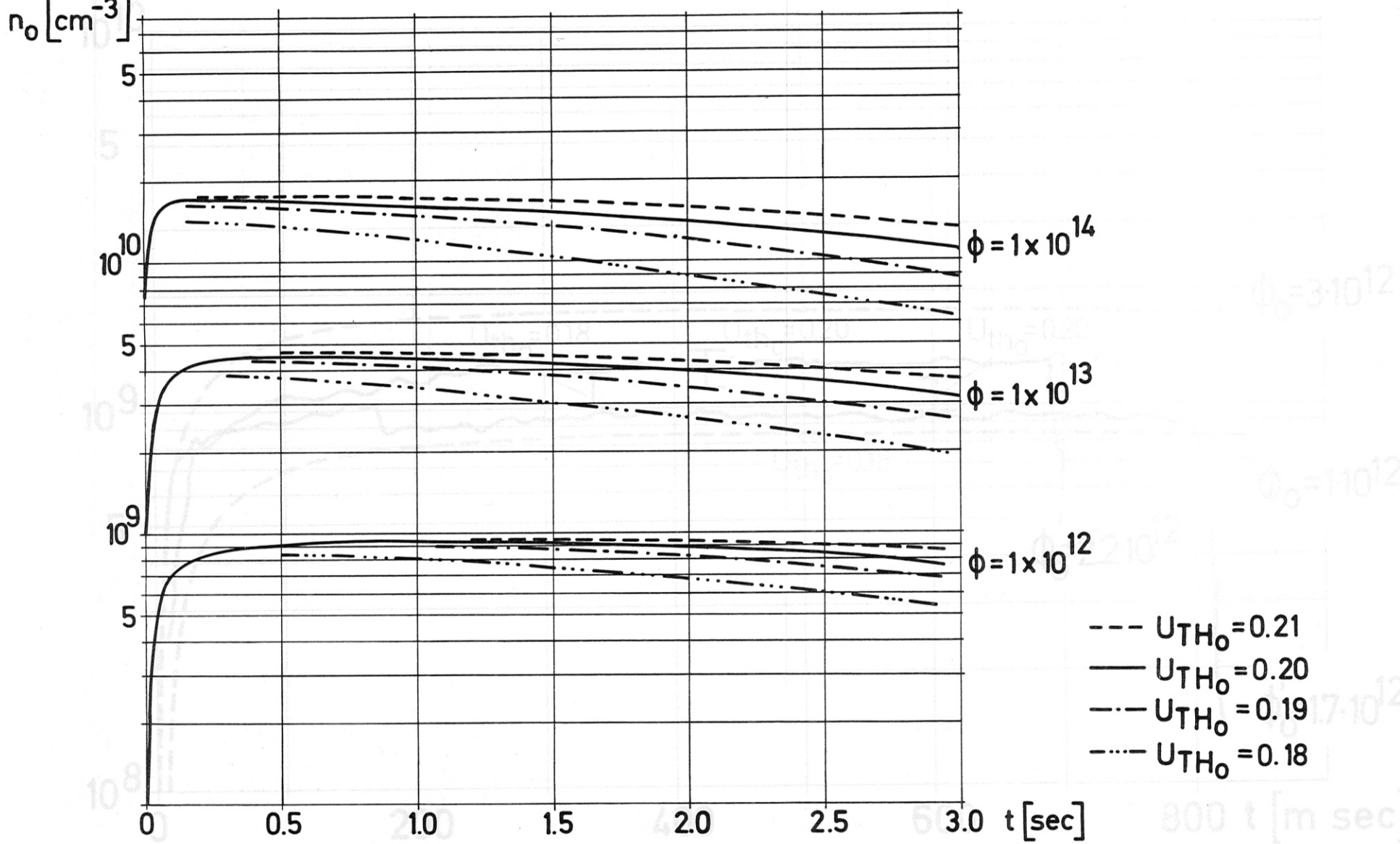
$n_o\,[cm^{-3}]$
5
10^{10}
5
10^{9}
5
$\phi = 1 \times 10^{14}$
$\phi = 1 \times 10^{13}$
$\phi = 1 \times 10^{12}$
$U_{TH_o} = 0.21$
$U_{TH_o} = 0.20$
$U_{TH_o} = 0.19$
$U_{TH_o} = 0.18$
0
0.5
1.0
1.5
2.0
2.5
3.0
t [sec]

Fig. 6

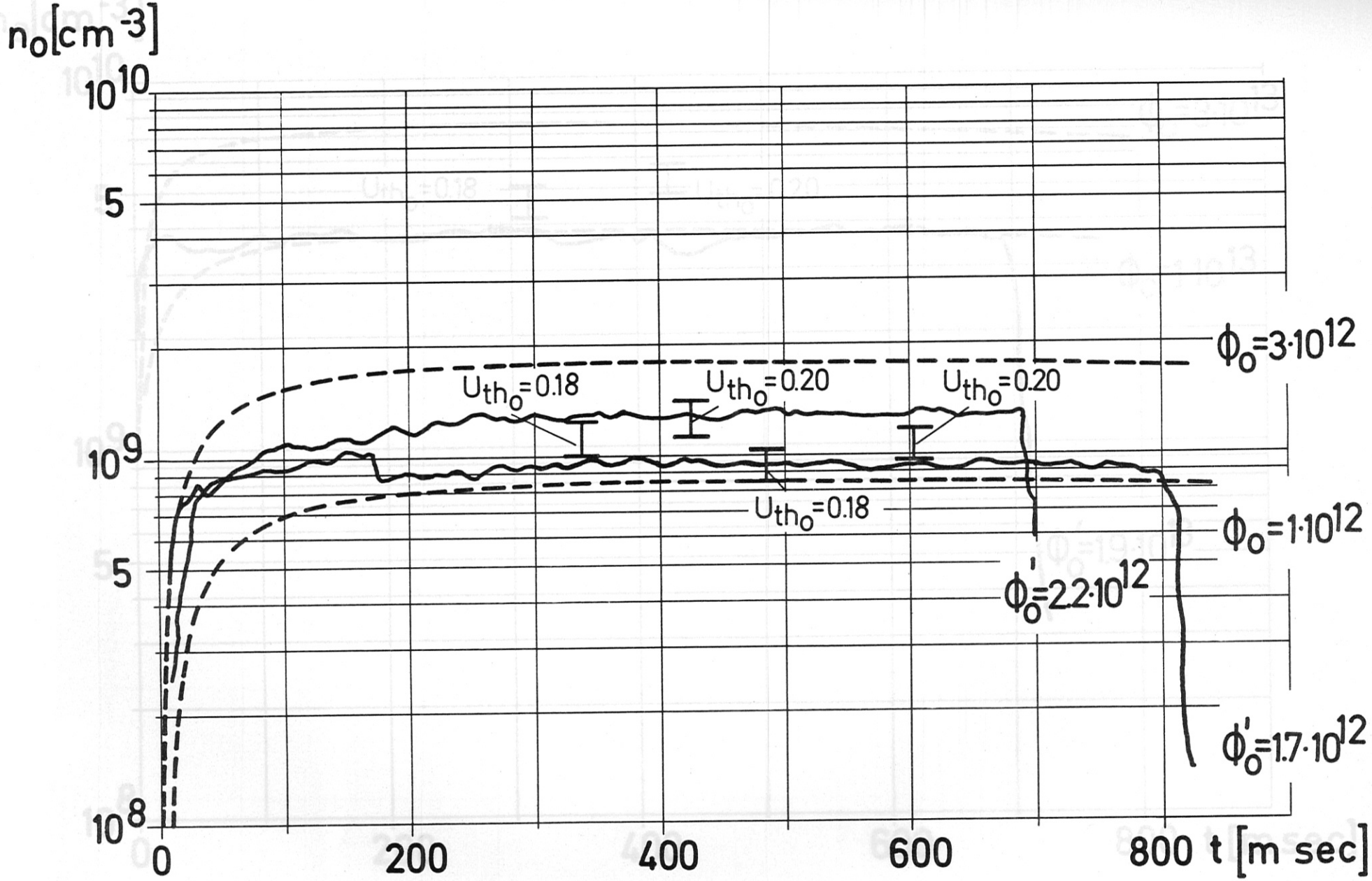
$n_o[cm^{-3}]$
10^{10}
5
10^9
5
10^8
0
200
400
600
800 t [m sec]
$\Phi_o=3\cdot10^{12}$
$\Phi_o=1\cdot10^{12}$
$\Phi_o'=2.2\cdot10^{12}$
$\Phi_o'=1.7\cdot10^{12}$
$U_{th_o}=0.18$
$U_{th_o}=0.20$
$U_{th_o}=0.20$
$U_{th_o}=0.18$

Fig. 7

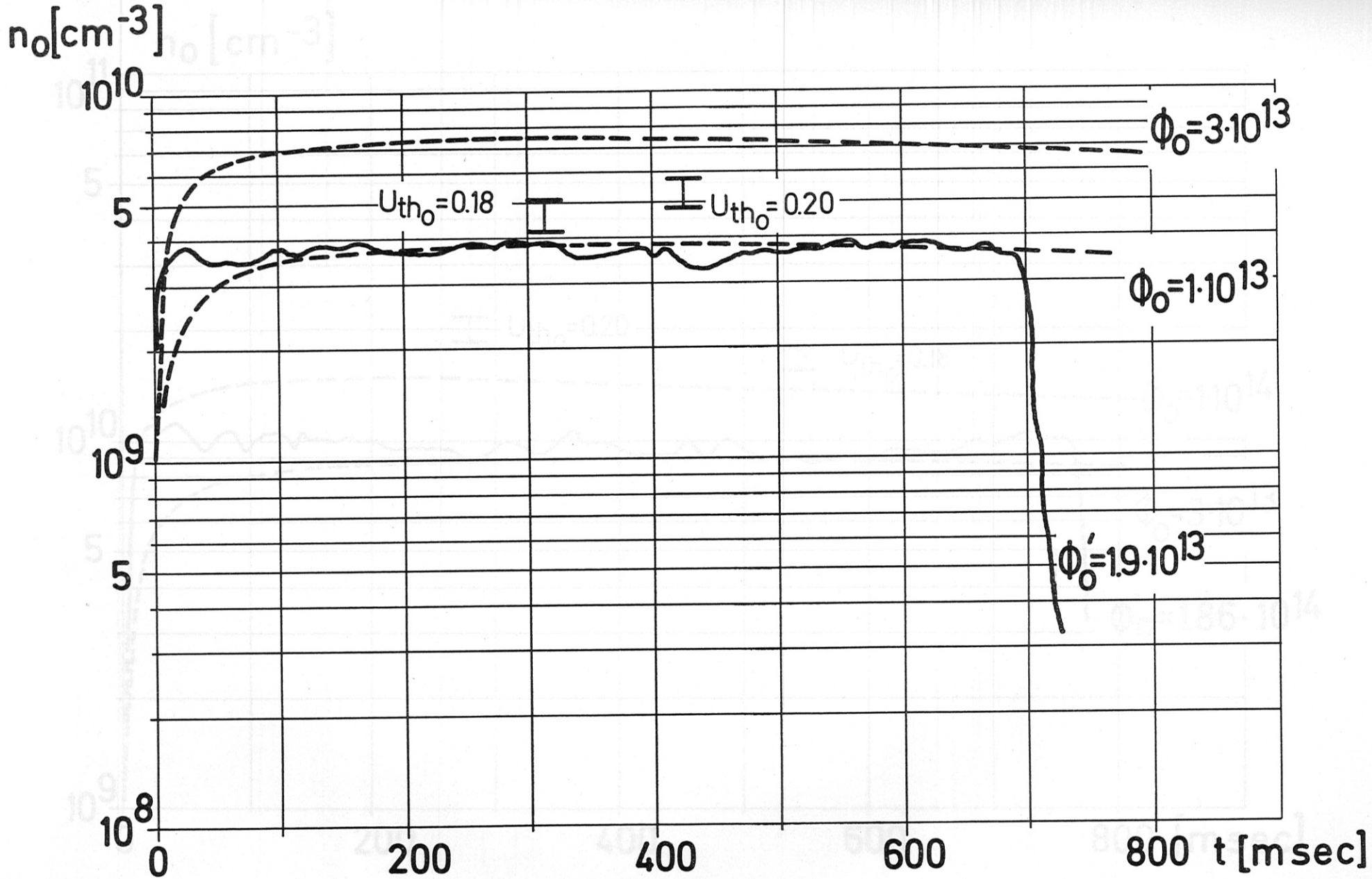
$n_o[cm^{-3}]$
10^{10}
5
10^9
5
10^8
0
200
400
600
800
t [msec]
$\Phi_o=3\cdot10^{13}$
$\Phi_o=1\cdot10^{13}$
$\Phi_o'=1.9\cdot10^{13}$
$U_{th_o}=0.18$
$U_{th_o}=0.20$

Fig.8

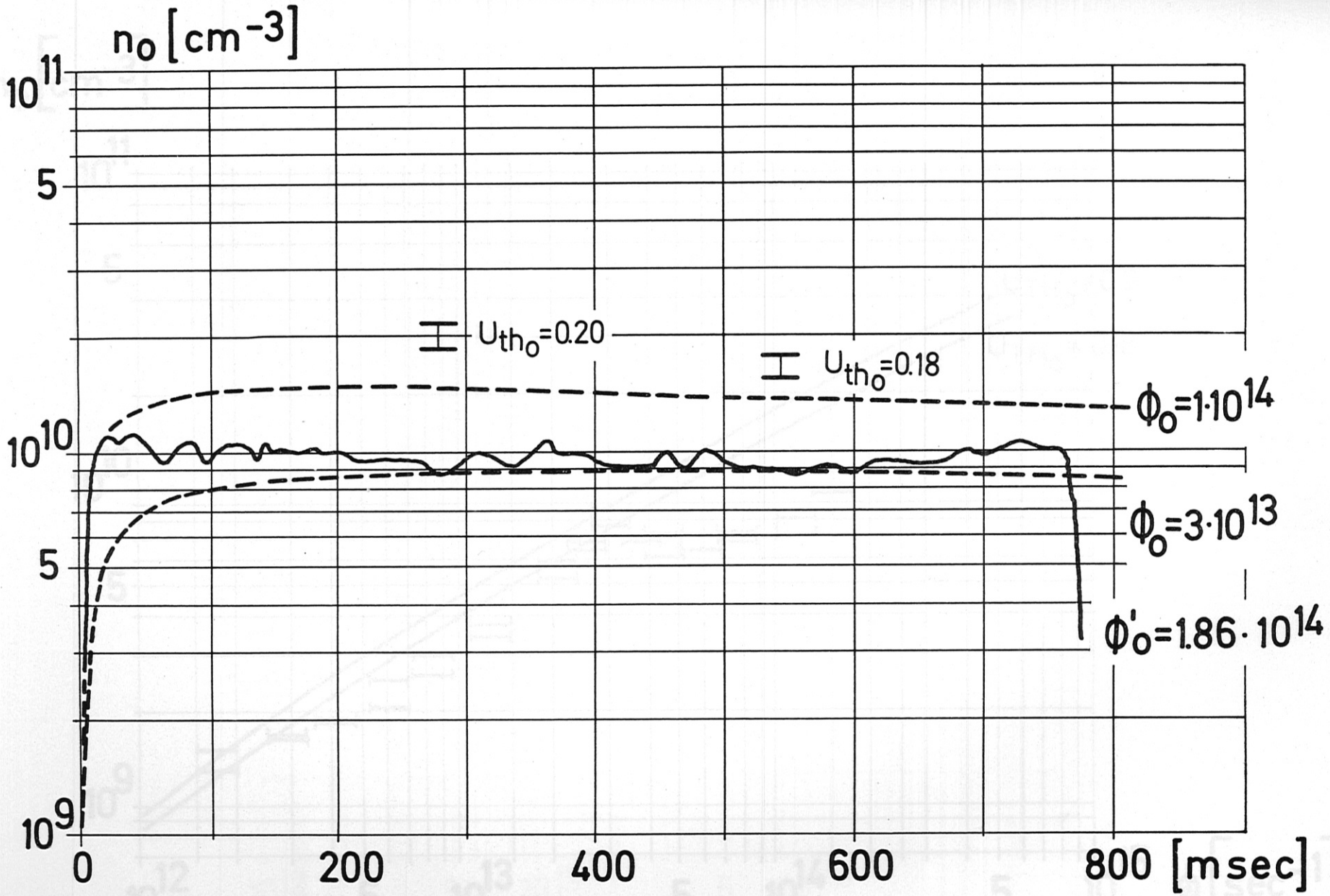
n_o [cm^{-3}]
10^{11}
5
10^{10}
5
10^9
U_{th_o}=0.20
U_{th_o}=0.18
ϕ_o=1·10^{14}
ϕ_o=3·10^{13}
ϕ'_o=1.86·10^{14}
0
200
400
600
800 [msec]

Fig. 9

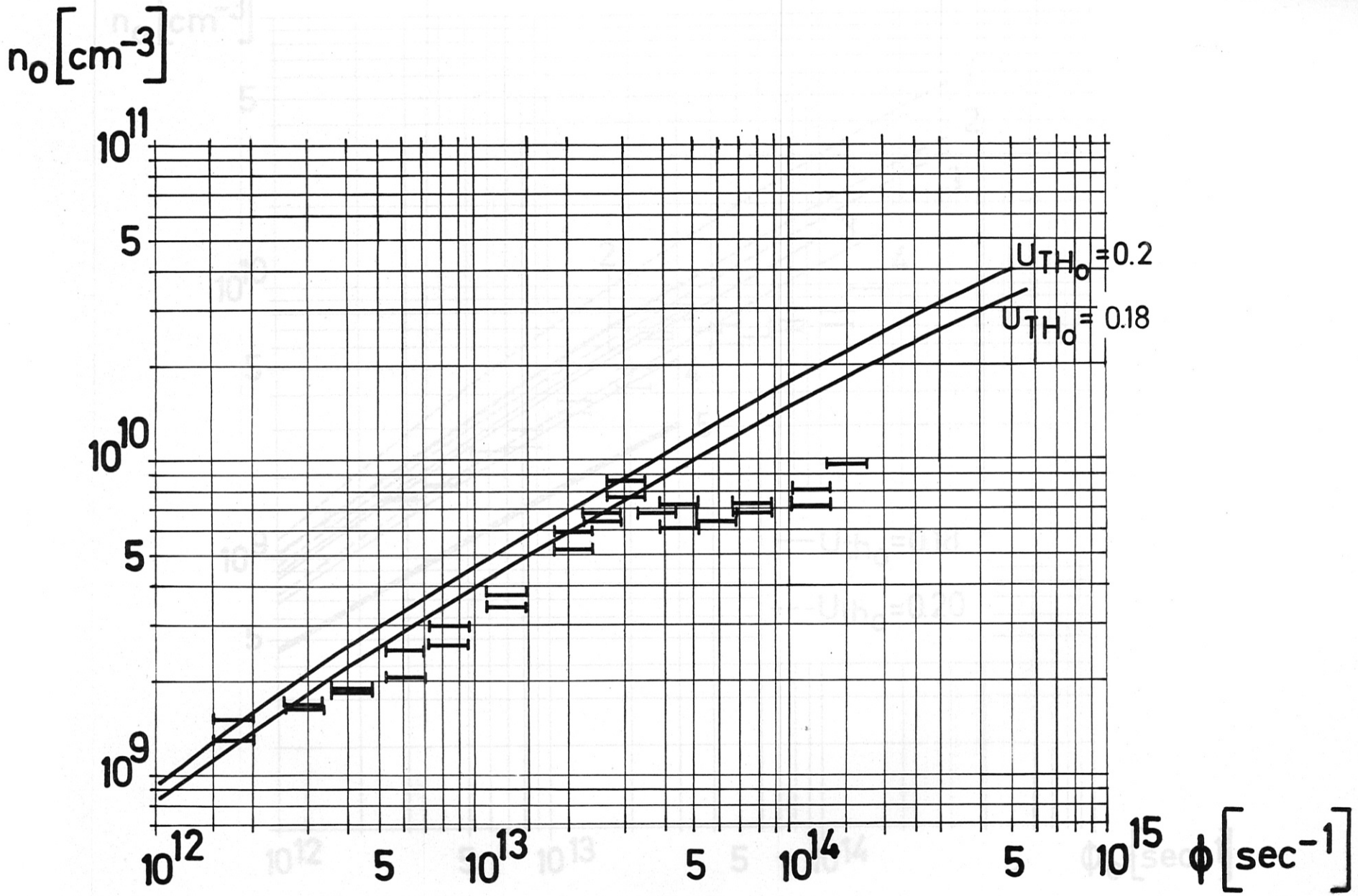
$n_o\left[cm^{-3}\right]$
10^{11}
5
10^{10}
5
10^9
$U_{TH_o}=0.2$
$U_{TH_o}=0.18$
10^{12}
5
10^{13}
5
10^{14}
5
10^{15}
$\phi\left[sec^{-1}\right]$

Fig. 10

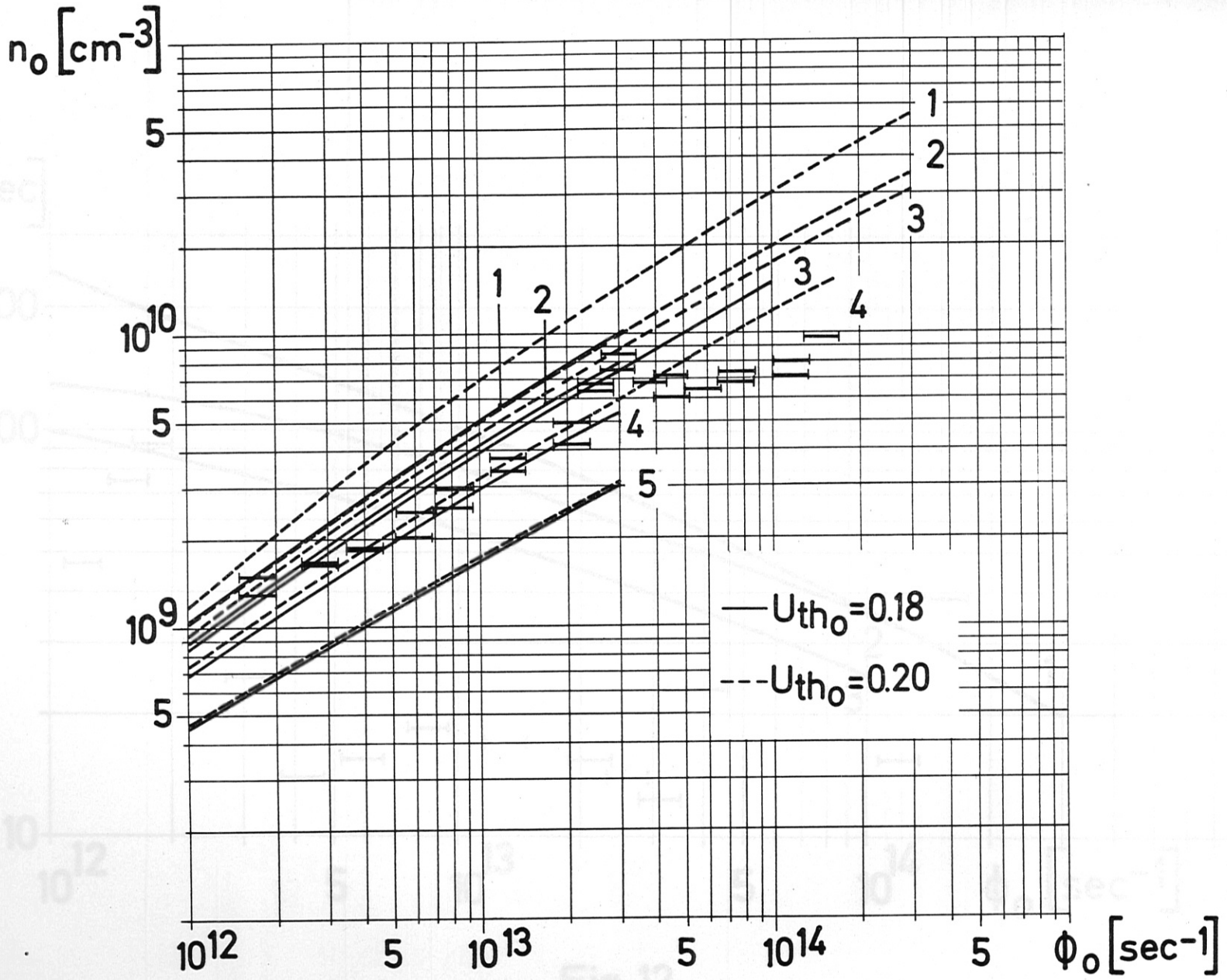
n_o [cm^{-3}]
5
10^{10}
5
10^9
5
10^{12}
5
10^{13}
5
10^{14}
5
Φ_o [sec^{-1}]
1
2
3
4
5
—U_{th_o}=0.18
---U_{th_o}=0.20

Fig. 11

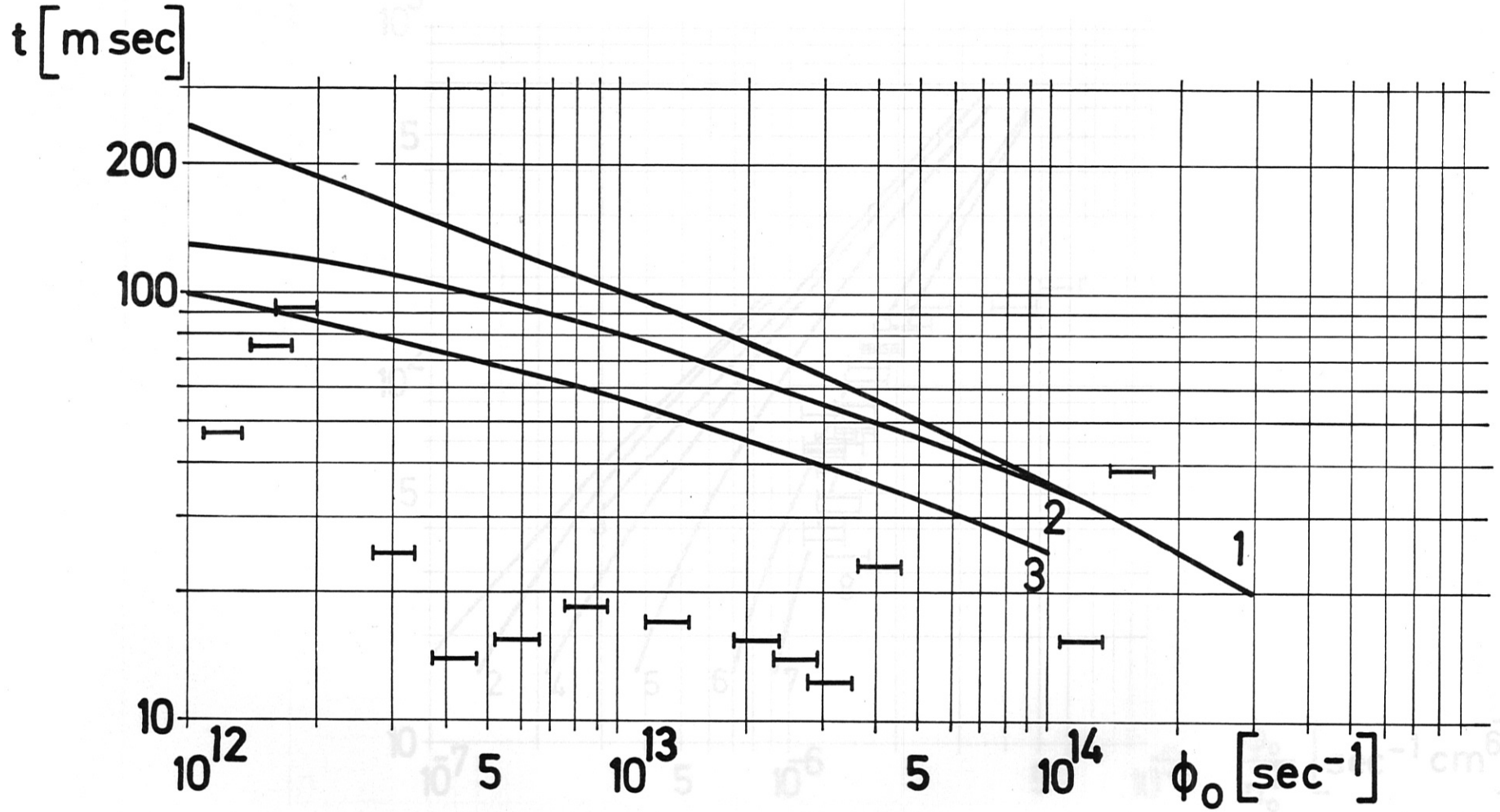

Fig.12

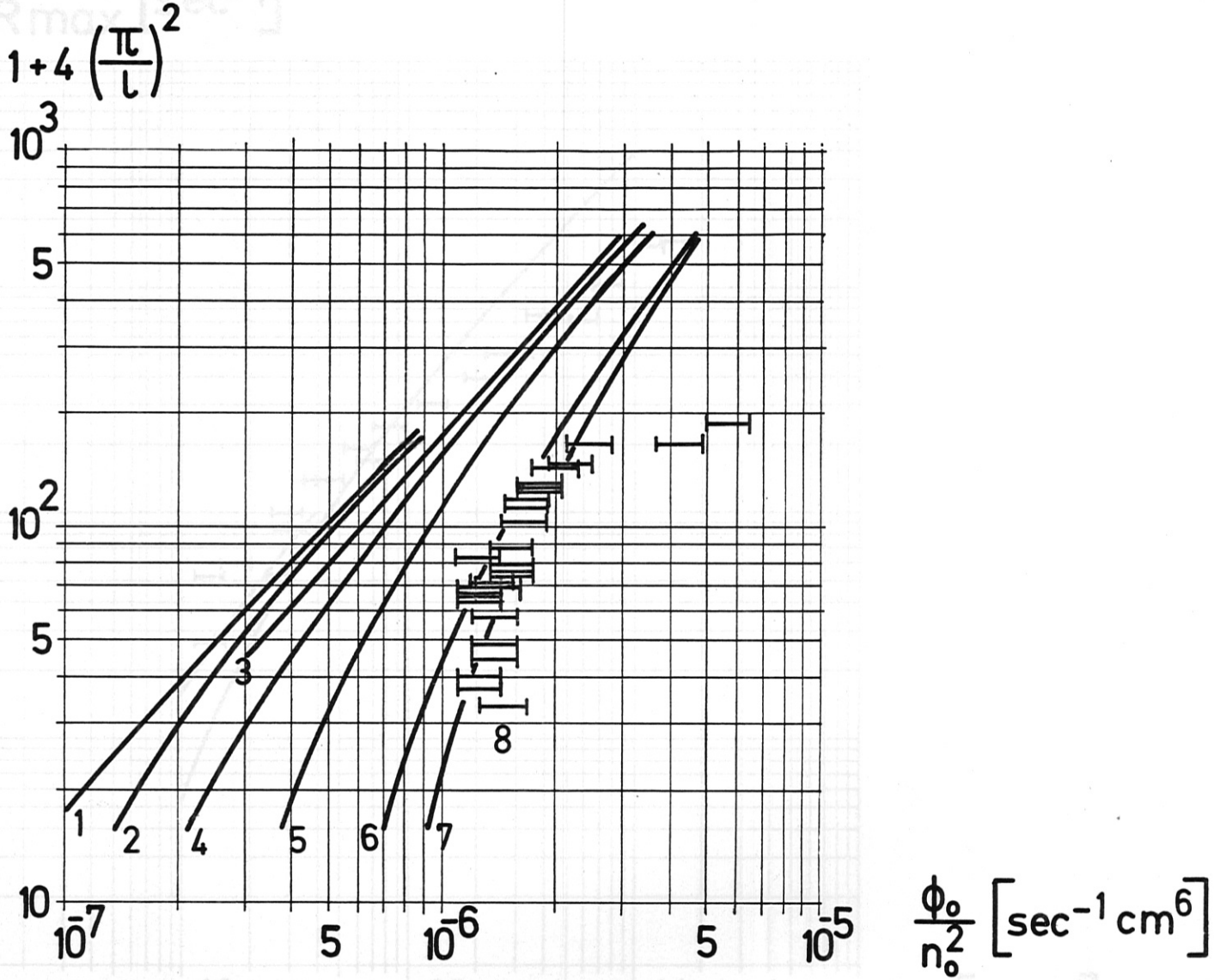
$1+4\left(\frac{\pi}{l}\right)^2$
10^3
5
10^2
5
10
1
2
3
4
5
6
7
8
10^{-7}
5
10^{-6}
5
10^{-5}
$\frac{\phi_o}{n_o^2}\left[\text{sec}^{-1}\,\text{cm}^6\right]$

Fig. 13

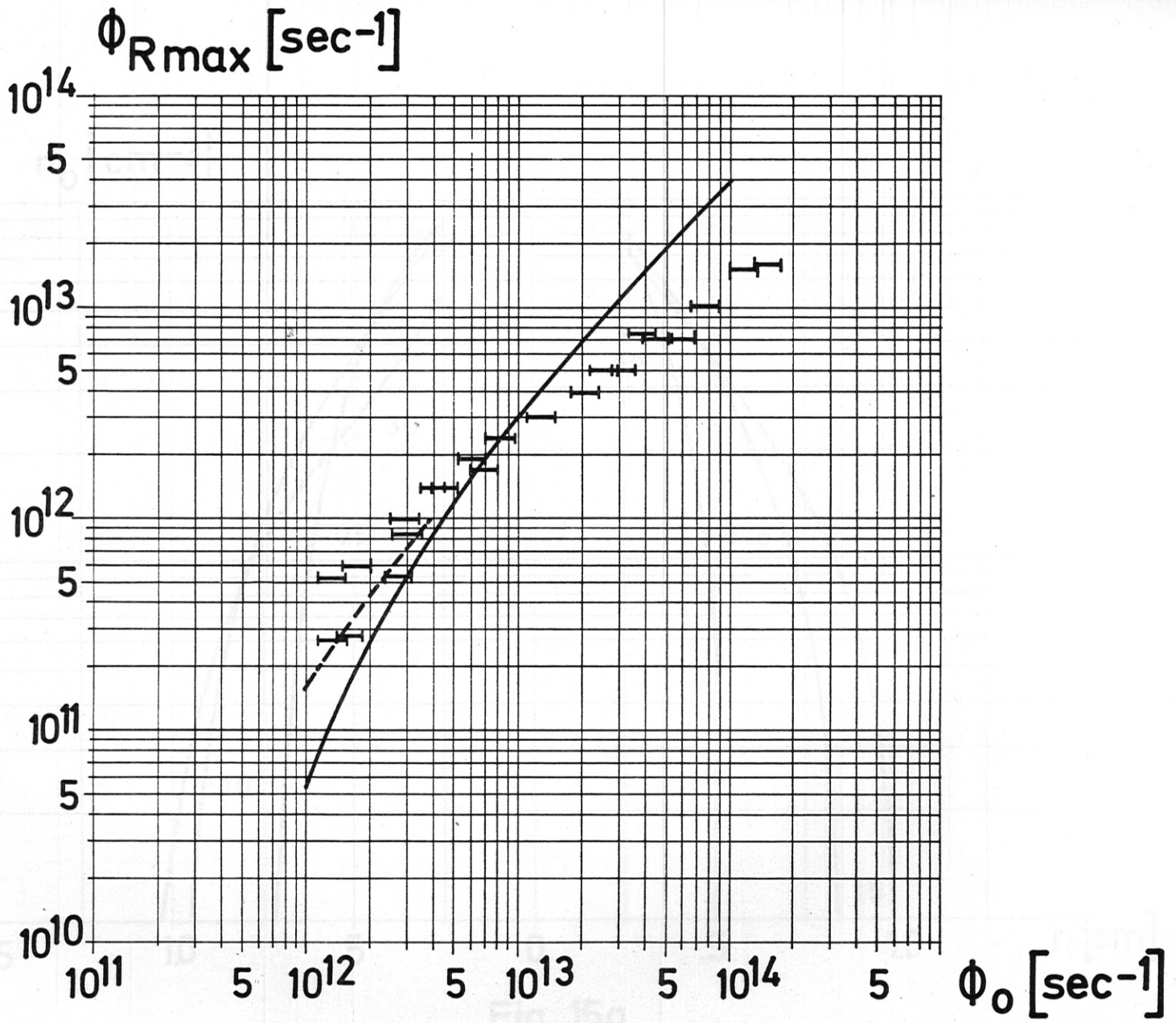
$\Phi_{R\,max}$ [sec^{-1}]
10^{14}
5
10^{13}
5
10^{12}
5
10^{11}
5
10^{10}
10^{11}
5
10^{12}
5
10^{13}
5
10^{14}
5
Φ_o [sec^{-1}]

Fig. 14

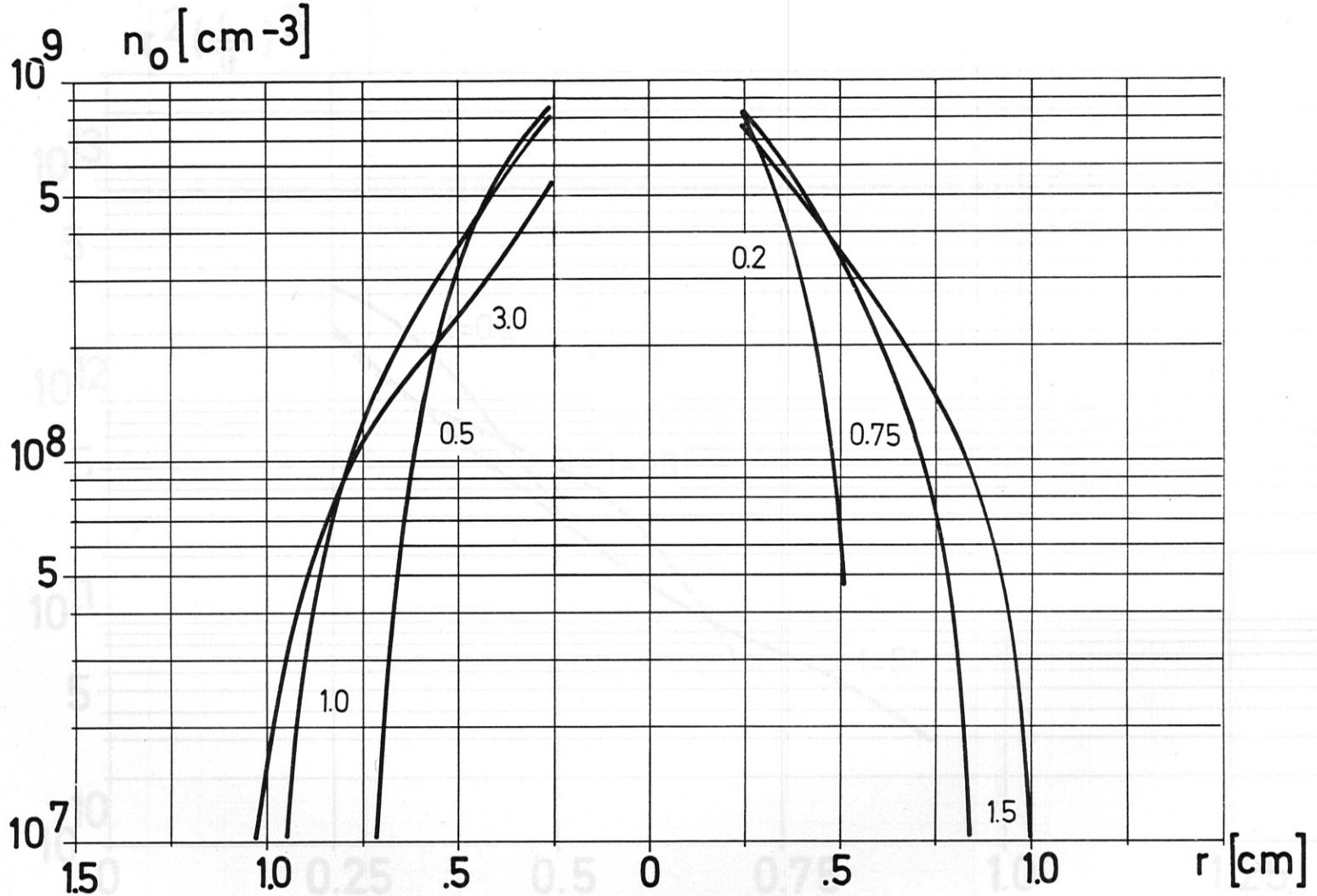

Fig. 15a

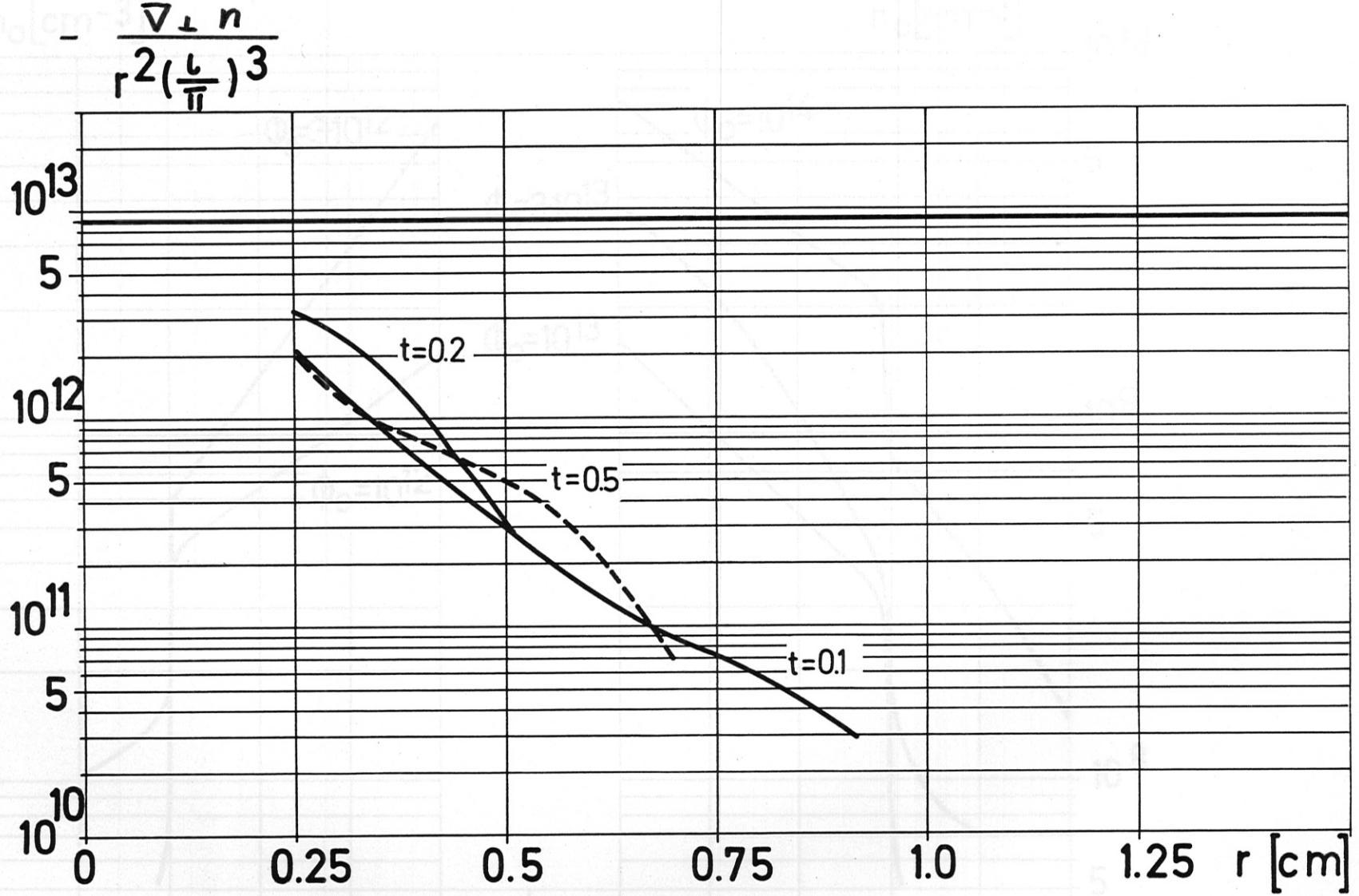
$-\frac{\nabla_\perp n}{r^2(\frac{L}{\pi})^3}$
10^{13}
5
10^{12}
5
10^{11}
5
10^{10}
t=0.2
t=0.5
t=0.1
0
0.25
0.5
0.75
1.0
1.25
r [cm]

Fig. 15b

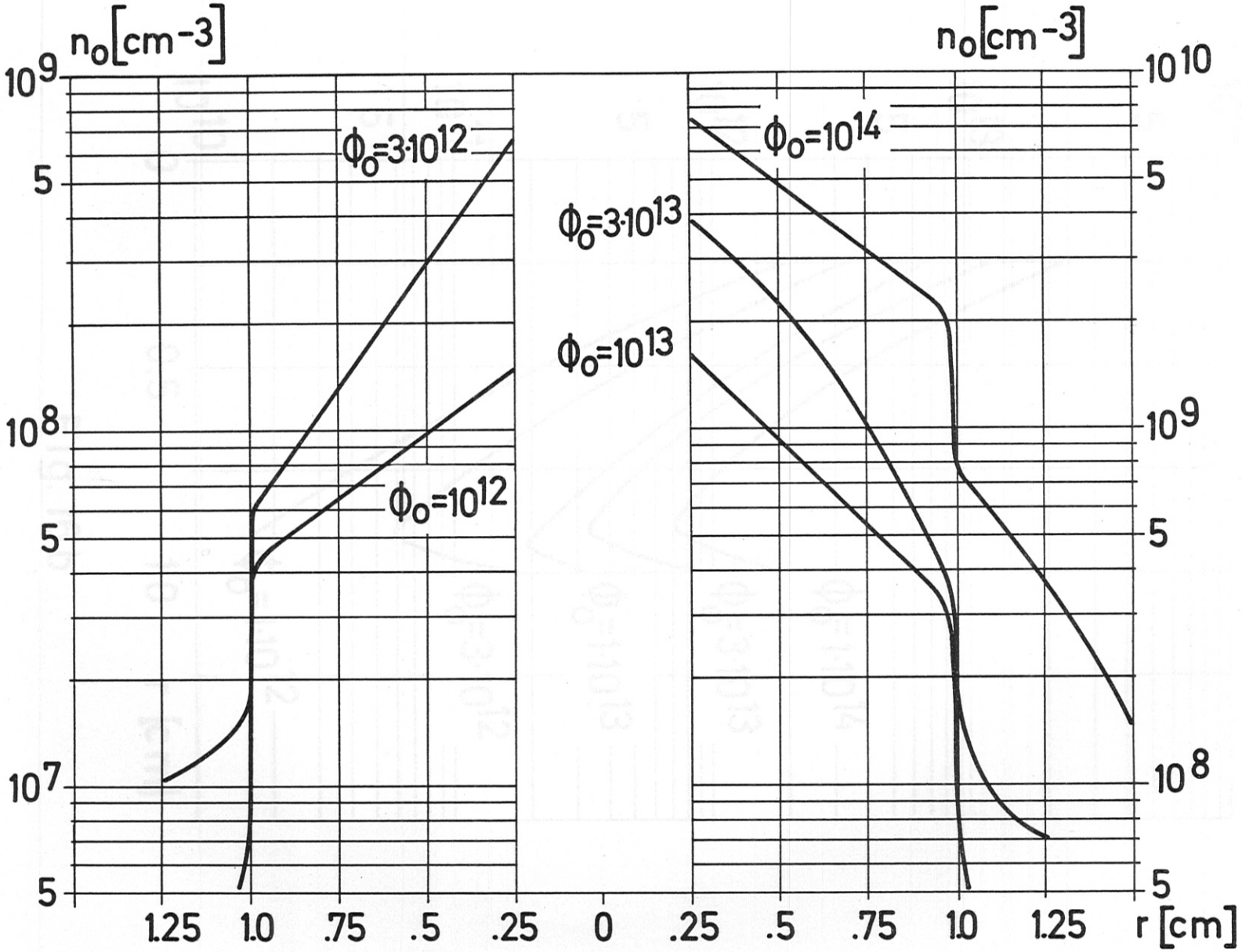
$n_o[cm^{-3}]$
10^9
5
10^8
5
10^7
5
$\phi_o=3\cdot10^{12}$
$\phi_o=10^{12}$
$\phi_o=3\cdot10^{13}$
$\phi_o=10^{13}$
$\phi_o=10^{14}$
$n_o[cm^{-3}]$
10^{10}
5
10^9
5
10^8
5
1.25
1.0
.75
.5
.25
0
.25
.5
.75
1.0
1.25
r [cm]

Fig. 16 a

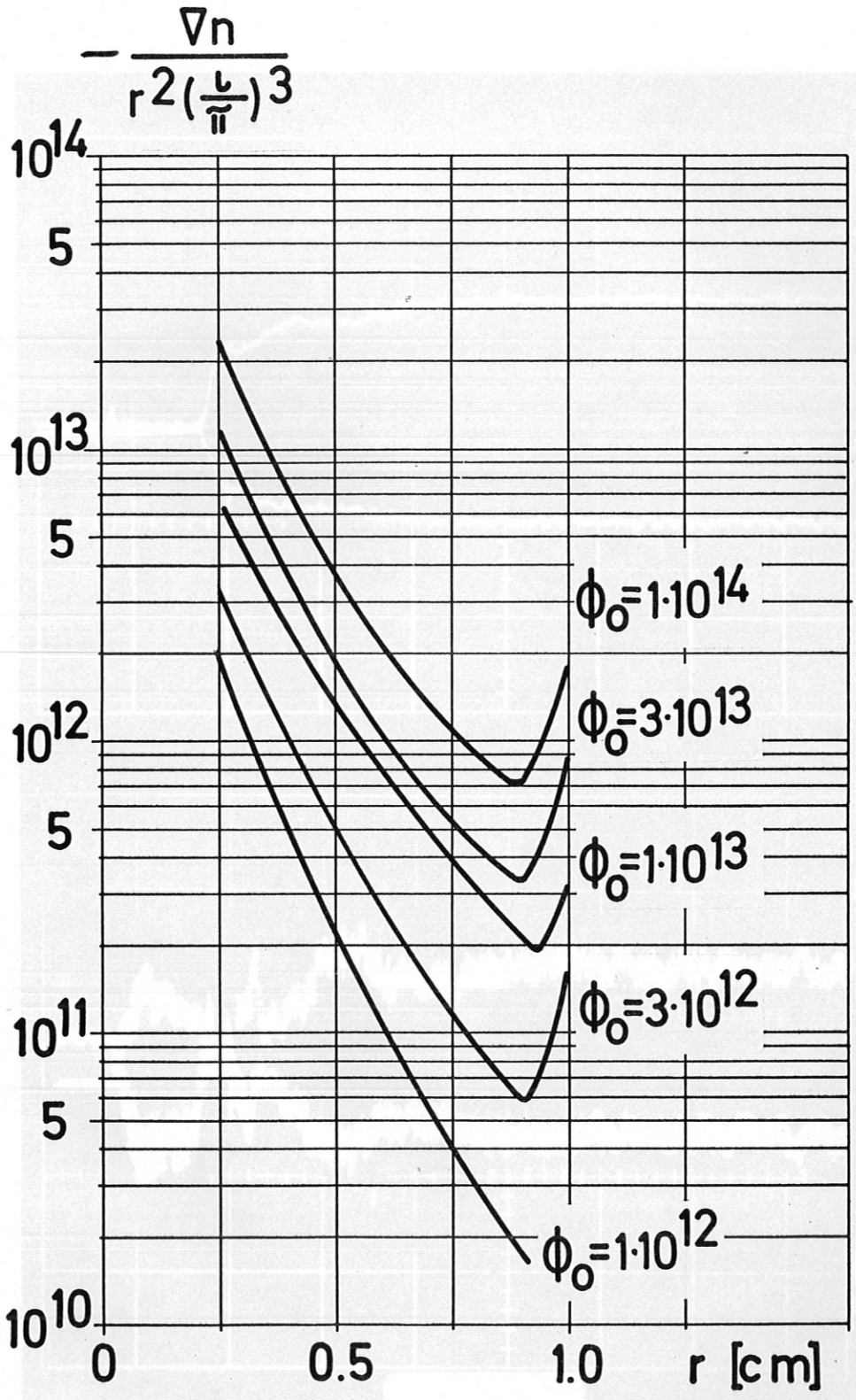
$-\frac{\nabla n}{r^2(\frac{\nu}{\pi})^3}$
10^{14}
5
10^{13}
5
10^{12}
5
10^{11}
5
10^{10}
$\phi_o=1\cdot10^{14}$
$\phi_o=3\cdot10^{13}$
$\phi_o=1\cdot10^{13}$
$\phi_o=3\cdot10^{12}$
$\phi_o=1\cdot10^{12}$
0
0.5
1.0
r [cm]

Fig. 16b

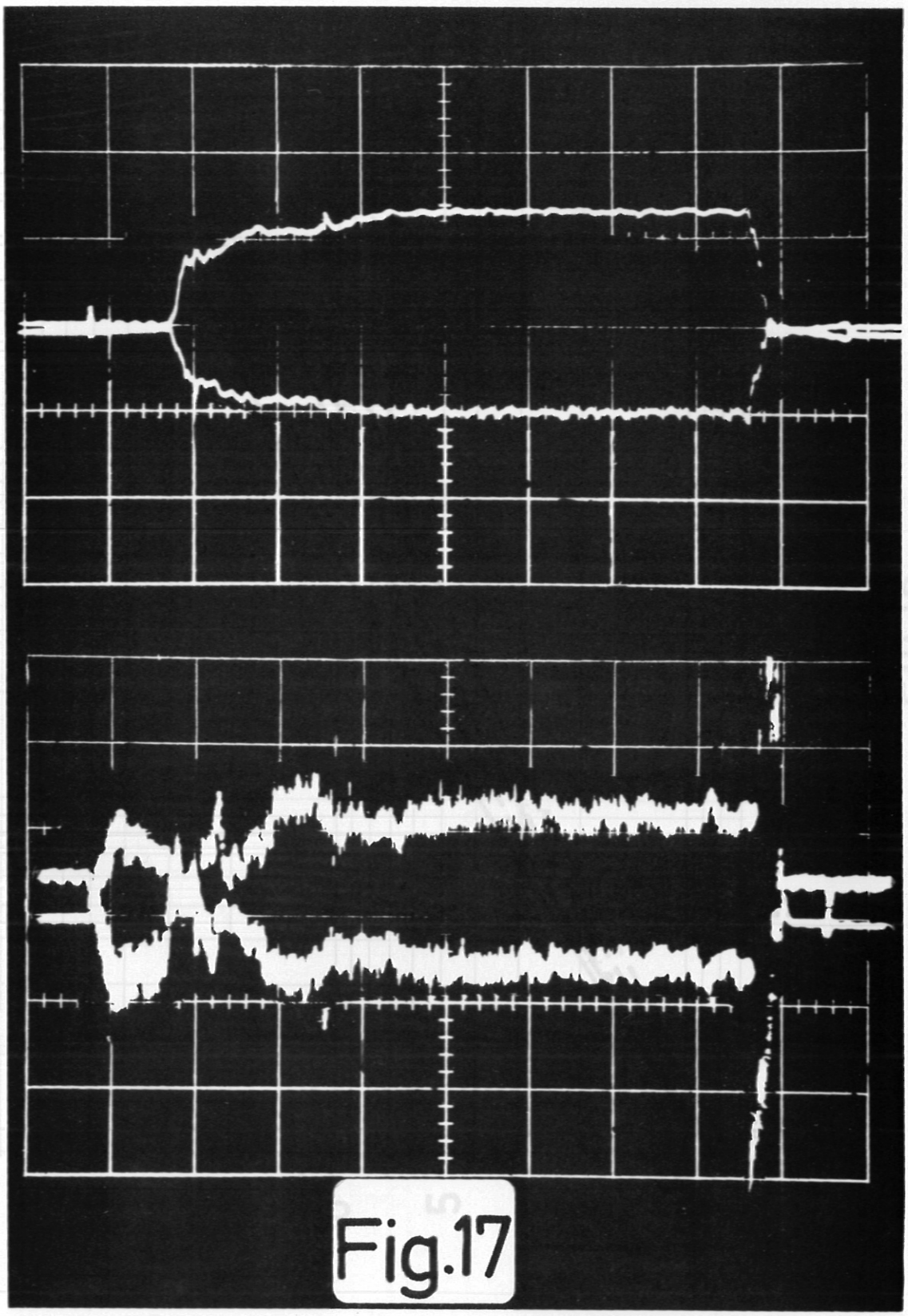

Fig.17

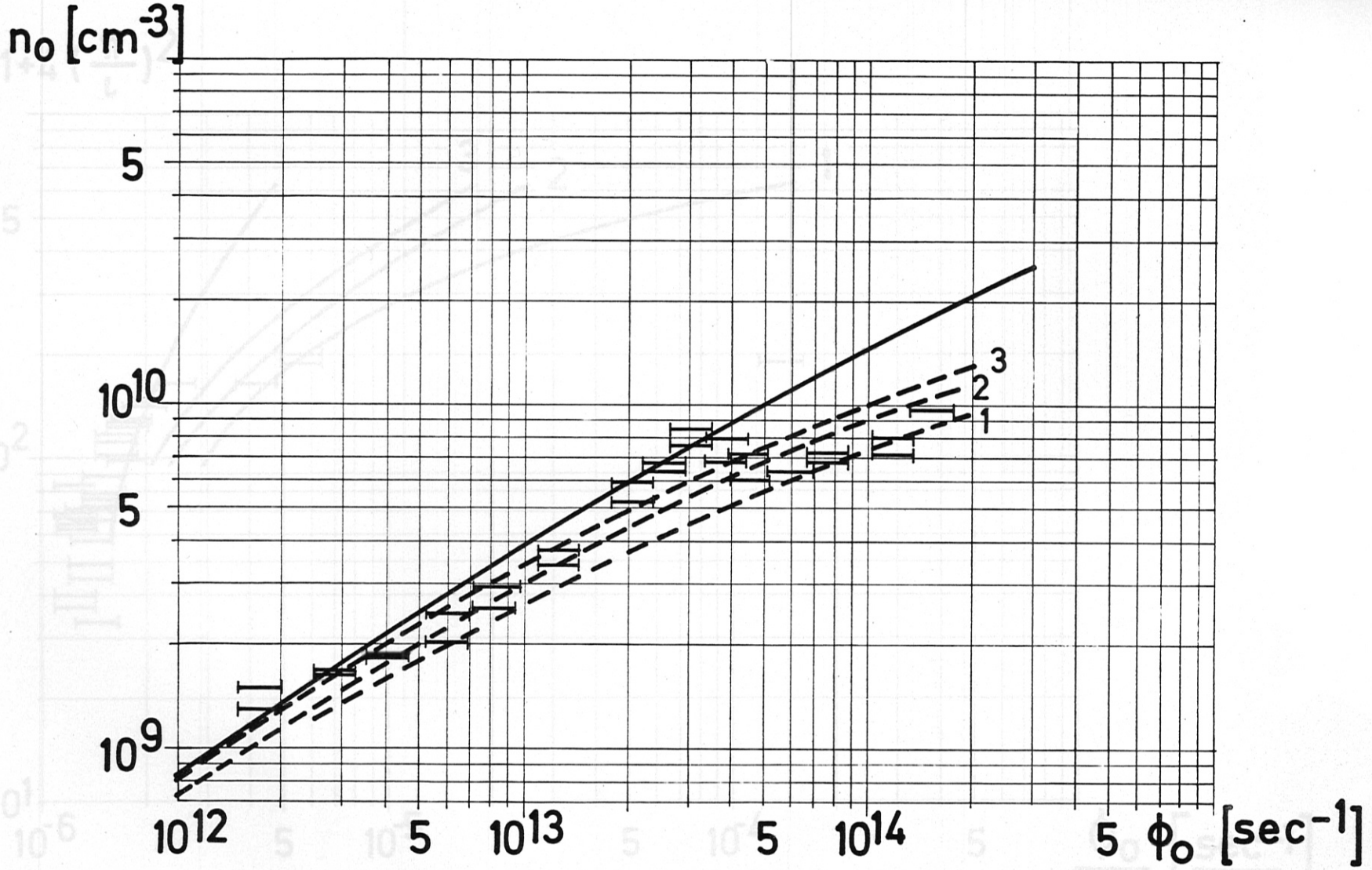

Fig. 18

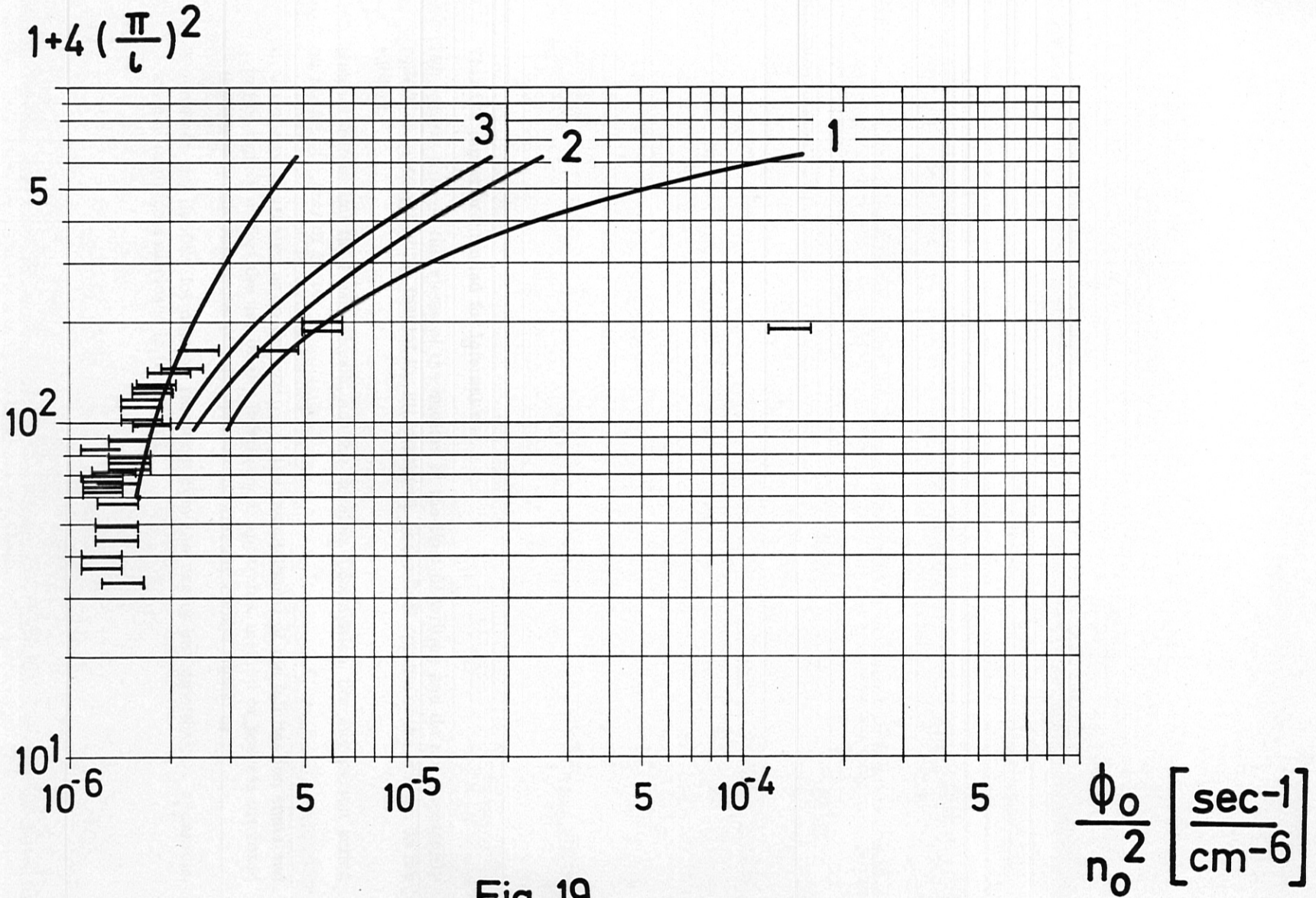
$1+4\left(\frac{\pi}{\iota}\right)^2$
5
10^2
10^1
10^{-6}
5
10^{-5}
5
10^{-4}
5
3
2
1
$\frac{\phi_o}{n_o^2}\left[\frac{sec^{-1}}{cm^{-6}}\right]$

Fig. 19